Research Square

Preprints are preliminary reports that have not undergone peer review.
They should not be considered conclusive, used to inform clinical practice,
or referenced by the media as validated information.

Targeting STAU1 ameliorates disease phenotypes in TDP-43 ALS mice

Daniel Scoles

daniel.scoles@hsc.utah.edu

University of Utah https://orcid.org/0000-0002-0583-4683

Sharan Paul

University of Utah

Warunee Dansithong

University of Utah

Karla P. Figueroa

University of Utah

Jinze Li

University of Utah

Pravin Hivare

University of Utah

Collin J. Anderson

University of Sydney

Mandi Gandelman

University of Utah

Stefan M. Pulst

University of Utah https://orcid.org/0000-0003-0883-7879

Research Article

Keywords: amyotrophic lateral sclerosis, dementia, ataxias, movement disorders, stau1, staufen1, antisense oligonucleotide

Posted Date: November 17th, 2026

DOI: https://doi.org/10.21203/rs.3.rs-11750300/v1

License: This work is licensed under a Creative Commons Attribution 4.0 International License.
Read Full License

Additional Declarations: The authors declare no competing interests.

Targeting STAU1 ameliorates disease phenotypes in TDP-43 ALS mice

Authors: Daniel R. Scoles[1,*], Sharan Paul[1], Warunee Dansithong[1], Karla P. Figueroa[1], Jinze Li[1], Pravin Hivare[1], Collin J. Anderson[1,†], Mandi Gandelman[1], Stefan M. Pulst[1,*].

Affiliations:
[1]Department of Neurology, University of Utah; Salt Lake City, UT, USA. 84132.
[†]Present Addresses: School of Medical Sciences, University of Sydney; Camperdown NSW 2006, Australia. School of Biomedical Engineering, University of Sydney; Darlington NSW 2008, Australia.

*Corresponding Authors. Emails: Stefan.Pulst@hsc.utah.edu, Daniel.Scoles@hsc.utah.edu.

ABSTRACT

Altered RNA metabolism and impaired proteostasis are central to amyotrophic lateral sclerosis (ALS) and frontotemporal dementia (FTD). STAU1 is a multifunctional RNA-binding protein that regulates mRNA decay and trafficking, interacts with ATXN2, and is overabundant in neurodegenerative disease models. STAU1 overabundance activates mTOR signaling, impairs autophagy and stress-granule turnover, and thereby participates in a feed-forward circuit that further elevates STAU1 abundance. Here, we tested whether genetic and antisense oligonucleotide (ASO)-mediated STAU1 lowering can interrupt this circuit in TDP-43-associated disease. *Stau1* haploinsufficiency in *Prp*-TDP-43^{Q331K} mice improved motor performance and open-field measures, reduced TDP-43 and gliosis, normalized neuronal, apoptotic, and autophagy markers, restored TDP-43-dependent splicing, and attenuated transcriptomic abnormalities. Screening 2′-*O*-methoxyethyl (MOE) gapmer ASOs identified ASO-45, which lowered STAU1 in patient-derived fibroblasts and mouse CNS. Intracerebroventricular ASO-45 improved spinal-cord and motor-cortex phenotypes, restored splicing, and attenuated cortical transcriptomic abnormalities. In independent *Thy1*-TDP-43 models, ASO-45 improved molecular markers and extended survival by 9.5–15.7%. These findings show that STAU1 lowering can disrupt a self-amplifying mTOR–autophagy–stress-granule axis and nominate STAU1-directed ASOs as a disease-modifying strategy for ALS/FTD.

INTRODUCTION

Disease-causing dominant variants in the *TARDBP* gene, encoding TDP-43, are associated with several neurodegenerative diseases, including amyotrophic lateral sclerosis (ALS) and frontotemporal dementia (FTD). Although *TARDBP* mutations are a relatively rare cause of ALS, cytoplasmic TDP-43 aggregates are found in 90–95% of spinal motor neurons from sporadic ALS patients. In sporadic as well as familial ALS, TDP-43 aggregates share similar core biochemical and morphologic features, including cytoplasmic mislocalization, hyperphosphorylation, ubiquitination, and formation of C-terminal fragments. Cytoplasmic aggregation is associated with reduced nuclear TDP-43 and RNA missplicing. Directly targeting *TARDBP* itself or the encoded protein is challenging because TDP-43 has essential functions in RNA metabolism. In the nucleus, it regulates RNA splicing and suppresses cryptic exon inclusion. In the cytoplasm, TDP-43 is involved in regulation of translation and mRNA transport and can localize to stress granules under certain conditions. Thus, it is not surprising that TDP-43 knockout in mice is embryonic lethal and conditional knockout in motor neurons leads to motor neuron death.

The essential functions of TDP-43 necessitate alternative strategies to modify its pathogenic effects. Lowering *ATXN2* expression has emerged as a compelling strategy, supported by evidence that ATXN2 reduction mitigates TDP-43 pathology and extends survival in ALS models [1]. These findings supported the development of antisense oligonucleotides (ASOs) targeting *ATXN2* [2], including BIIB105, which advanced to early-phase clinical testing [3] but was halted due to lack of clinical efficacy.

As *ATXN2* reduction showed promise ALS models, we explored whether other proteins in the ATXN2/RNA complex might provide therapeutic targets and identified STAU1. STAU1 is a double-stranded RNA binding protein that functions in RNA degradation, mRNA trafficking in neurons, and mRNA nuclear exit. STAU1 interacts with wild-type and polyQ-expanded ATXN2 but is greatly overabundant in SCA2 patient-derived cells [4, 5]. Subsequent studies demonstrated that this overabundance was post-transcriptional and due to reduced autophagic degradation. Mechanistically, STAU1 directly interacts with the 5'-UTR of *MTOR* mRNA, resulting in increased mTOR translation and reduced autophagy [6, 7]. STAU1 overabundance is associated with abnormal autophagy in multiple human tissues and mouse models of neurodegenerative disease [4, 5, 6]. These mechanisms were not limited to SCA2 cells but were also present in other neurodegenerative diseases, including Huntington's disease (HD), C9ORF72 ALS, and TDP-43 ALS [4, 5, 6]. Of note, spinal cords from patients with C9ORF72 ALS and sporadic sporadic ALS had overabundant STAU1 [5]. Reducing STAU1 abundance normalized autophagy markers, abnormal UPR activation, and abnormal p53-signaling in several neurodegenerative in vitro and in vivo model systems [4, 5, 6]. Together, these findings suggest that reducing STAU1 expression may represent a novel therapeutic strategy for familial and sporadic ALS.

Here we first provide genetic proof-of-concept that lowering STAU1 in an ALS mouse model ameliorates motor, molecular, histological, and TDP-43-dependent splicing phenotypes. We then describe the development of an antisense oligonucleotide (ASO) therapeutic targeting *STAU1*. We further show that lowering *STAU1* modifies mTOR-related autophagy phenotypes in cultured cells and in a BAC-*hSTAU1* transgenic mouse model [8]. Finally, we identified ASOs targeting mouse *Stau1* suitable for proof-of-concept studies and demonstrate improved neuronal phenotypes in two TDP-43 transgenic mouse models, including improved survival.

RESULTS

Genetic reduction of *Stau1* ameliorates TDP-43–associated phenotypes in vivo

To determine the effects of genetically lowering STAU1 abundance in TDP-43 transgenic mice, we crossed *Prp*-TDP43^{Q331K} mice [9] with *Stau1*$^{+/-}$ mice [10], producing 4 genotypes of mice for testing: wildtype (WT), *Stau1*$^{+/-}$, *Prp*-TDP43^{Q331K}, and *Prp*-TDP43^{Q331K};*Stau1*$^{+/-}$. At prespecified time points, mice underwent longitudinal motor testing, including rotarod, grip-strength, and clasping assessments, followed by a terminal open-field test. At the study endpoint, mice were euthanized and CNS tissues were collected for Western blotting, reverse transcription (RT)-PCR, and immunofluorescence analyses. A summary of the genetic interaction study is shown in Fig. 1A.

Stau1 haploinsufficiency improves motor phenotypes in *Prp*-TDP43^{Q331K} mice

Mice were assessed on an accelerating rotarod at 8, 12, 16, and 20 weeks of age. At each time point, *Prp*-TDP43^{Q331K} mice exhibited significantly reduced latency to fall relative to WT and *Stau1*$^{+/-}$ mice. This deficit was significantly ameliorated in *Prp*-TDP43^{Q331K};*Stau1*$^{+/-}$ mice (Fig. 1B). Male mice weighed significantly more than female mice across all genotype groups; however, body weight did not differ among genotype groups within either sex (Supplementary Fig. 1A,B). Both sexes were included in the rotarod analysis, and performance was not adjusted for body weight. Sex-stratified rotarod data showed a generally similar pattern to the pooled analysis (Supplementary Fig. 1C).

Forelimb and hindlimb grip strength were assessed at 14 and 18 weeks of age. At both time points, *Prp*-TDP43^{Q331K} mice showed significantly reduced forelimb and hindlimb grip strength relative to WT and *Stau1*$^{+/-}$ mice; these deficits were significantly improved in *Prp*-TDP43^{Q331K};*Stau1*$^{+/-}$ mice (Fig. 1C). Clasping behavior was assessed at 12, 16, and 20 weeks of age. Clasping was not observed in WT or *Stau1*$^{+/-}$ mice. In contrast, *Prp*-TDP43^{Q331K} mice exhibited elevated mean clasping scores at each time point, which were significantly reduced in *Prp*-TDP43^{Q331K};*Stau1*$^{+/-}$ mice (Supplementary Fig. 1D).

Mice were assessed in the open-field test at 21 weeks of age. A heatmap of regional dwell time showed that *Prp*-TDP43^{Q331K} mice spent less time in the central zone than all other groups (Fig. 1D), consistent

with anxiety-like behavior. Three quantitative measures—total distance traveled, number of entries into the central zone, and distance traveled in the central zone—were each reduced in *Prp*-TDP43^{Q331K} mice relative to the other groups. These phenotypes were significantly ameliorated in *Prp*-TDP43^{Q331K};*Stau1*$^{+/-}$ mice (Fig. 1E). In addition, absolute head-turn angle, an exploratory-behavior measure, was reduced in *Prp*-TDP43^{Q331K} mice and significantly increased in *Prp*-TDP43^{Q331K};*Stau1*$^{+/-}$ mice (Supplementary Fig. 1E).

Stau1 haploinsufficiency ameliorates molecular and histological abnormalities in *Prp*-TDP43^{Q331K} mice

At 22 weeks of age, at the endpoint of the genetic interaction study, mice were euthanized and spinal cord lysates were evaluated for molecular abnormalities. Western blotting revealed an abnormal molecular phenotype in *Prp*-TDP43^{Q331K} mice, including elevated levels of autophagy-related proteins (mTOR and p62), reduced neuronal markers (NeuN and ChAT), elevated GFAP consistent with gliosis, and increased cleaved caspase-3 (cCASP3), a marker of cell death. These abnormalities were restored to levels comparable to those in WT and *Stau1*$^{+/-}$ mice in *Prp*-TDP43^{Q331K};*Stau1*$^{+/-}$ mice (Fig. 2A,B). In addition, *Prp*-TDP43^{Q331K};*Stau1*$^{+/-}$ mice exhibited significantly reduced spinal cord human TDP-43 (hTDP-43) abundance relative to *Prp*-TDP43^{Q331K} mice, consistent with reduced TDP-43 accumulation following genetic reduction of *Stau1*.

To determine whether the reduction in spinal cord TDP-43 abundance reflected changes in motor neurons, we performed immunofluorescent labeling with a human TDP-43–specific antibody and quantified signal within regions of interest encompassing individual motor neurons. *Prp*-TDP43^{Q331K};*Stau1*$^{+/-}$ mice exhibited significantly reduced motor-neuron TDP-43 immunoreactivity relative to *Prp*-TDP43^{Q331K} mice (Fig. 2C,D).

Stau1 haploinsufficiency restores TDP-43–dependent splicing in *Prp*-TDP43^{Q331K} mice

To determine whether genetic reduction of *Stau1* modifies TDP-43–regulated RNA processing, we examined alternative splicing of *Sort1*, two *Kcnip2* splice variants, and *Ahi1* in spinal cord. These events were previously identified as TDP-43^{Q331K}-associated alternative-splicing abnormalities in this transgenic mouse model [9]. We observed these events in spinal cord of both 4 month old *Prp*-TDP-43^{Q331K} mice and 12 month old BAC-STAU1 mice (Supplementary Fig. 3A-D). We confirmed abnormal splicing ratios for all three transcripts in *Prp*-TDP43^{Q331K} mice relative to WT and *Stau1*$^{+/-}$ mice; *Stau1* haploinsufficiency significantly ameliorated the abnormal splicing of *Sort1*, both *Kcnip2* splice variants, and *Ahi1* in *Prp*-TDP43^{Q331K};*Stau1*$^{+/-}$ mice (Fig. 2E–G). These findings demonstrate that genetic reduction of *Stau1* ameliorates previously described TDP-43^{Q331K}-associated splicing abnormalities in vivo.

Identification of lead *STAU1* ASOs

We designed 3,664 20-mer ASOs spanning the STAU1 5′- and 3′-UTRs. Candidates with ≥4 consecutive Gs, 40–60% GC content outside the target range, or absent cynomolgus alignment were excluded. We synthesized 118 spaced ~10 bp apart as fully phosphorothioated 5-10-5 2′-*O*-methoxyethyl gapmers with 5′-methylcytosines. Two also targeted mouse *Stau1* (ASO-45 and ASO-308). In HEK-293 cells, 118 ASOs were screened at 50 nM for 48 h; ASO-249 was most efficacious and ASO-45 ranked third (Supplementary Fig. 4A).

The most efficacious 37 ASOs from the HEK-293 screen in SCA2 (Q22/Q45) were screened in patient fibroblasts, along with ASO-239 that was least effective in HEK-293 cells as a non-targeting negative control. Cells were transfected at 100 nM in triplicate for 48 hours. The maximum *STAU1* reduction was 98.6% for ASO-276 and ASO-45 ranked 8th (Supplementary Fig. 4B).

Dose-response curves for the 21 most efficacious ASOs were determined in SCA2 (Q22/Q45) fibroblasts. ASO-45 was included in each batch to assess reproducibility. Across five batch sets, its IC50 varied by only ±2.2 nM; ASO-308 had the lowest IC50 among the 21 ASOs (Supplementary Figs. 4C and 5).

Alignment of the most efficacious ASOs to GRCh38/hg38 identified potential off-targets for several candidates, including *SORL1* for ASO-308 and ASO-287, *FUT8* and *PARD3B* for ASO-294, and *POLG2* for ASO-278. These ASOs were not advanced, except ASO-308 for comparison with ASO-45 in WT mice. ASO-45 had one predicted human off-target, *MCTS1* (94% identity), and no predicted mouse off-targets by alignment to MM10.

To characterize efficacy for the remaining 10 most potent ASOs for normalization of pathologically elevated STAU1, we utilized CRISPR-Cas9 edited HEK-293 cells expressing polyglutamine expanded ATXN2 (ATXN2-Q58 KI cells), that have elevated STAU1 abundance [4, 5]. Transfection of each of the 10 lead ASOs significantly lowered STAU1 levels to quantities equal to that in the parental HEK-293 cells (Supplemental Fig. 6).

***In vivo* ASO screening**

Evaluation of ASOs *in vivo* was made possible by our prior production of the BAC-STAU1 mouse harboring the human *STAU1* gene. BAC-STAU1 mice express an increased abundance of STAU1 protein in cerebral hemispheres, cerebellum and spinal cord associated with increased levels of autophagy signaling pathway proteins including mTOR, hyperphosphorylated mTOR, p62, and LC3-II [8]. BAC-STAU1 mice also displayed reduced levels of *Calb1, Rgs8, Pcp2, Pcp4* and *Fam107b* in cerebellum [8]. We evaluated efficacy for the 10 most potent lead ASOs in BAC-STAU1 mice. We treated 8 wk old BAC-STAU1 mice by intracerebroventricular (ICV) injection of 300 μg ASO for 2 wks and evaluated

cerebellar proteins on western blots. Each of the ASOs significantly reduced STAU1 abundance (Supplementary Fig. 7). Additionally, for all ASOs the abnormally elevated levels of GFAP, mTOR, p62, and LC3-II were significantly reduced, and abnormally reduced CALB1, was significantly increased in cerebellum (Supplementary Fig. 7).

We next assessed acute tolerability and gliosis markers in BAC-STAU1 mice. After 300 µg ICV ASO for 2 weeks, two mice were lost in the ASO-288 and ASO-310 groups, and one in the ASO-322 group; ASO-307 increased Aif1 (Supplementary Fig. 8). Five ASOs were advanced to dose-dependent testing: ASO-256, -319, -249, -270, and -45. Eight-week-old mice received 300, 600, or 900 µg ASO ICV for 2 weeks (n = 3/group). Toxicity increased with dose for some ASOs, with complete mortality at 900 µg ASO-249 or ASO-319. All ASOs reduced STAU1; Aif1 and Gfap were not increased except by ASO-256 (Supplementary Fig. 8).

The work described above resulted in the identification of 5 lead ASOs including ASOs 45, 249, 256, 270 and 319. Supplementary Fig. 9 illustrates the position of all ASOs screened in the study, their positions among the STAU1 exons, and their efficacy in the primary screen. The positions of the five lead ASOs are indicated, as well as that for ASO-308, that like ASO-45 also targets mouse *Stau1*.

ASOs targeting mouse *Stau1*

Our ASO screen identified two ASOs that target human *STAU1* that also have sequence identity to mouse *Stau1*, ASO-45 and ASO-308. To compare their efficacy, we treated 11 wk old wildtype mice with 500 µg ASO by ICV injection with 2 wk treatment time. At the endpoint we evaluated cerebellar proteins on western blots demonstrating ~70% reduction of STAU1 protein levels compared to PBS treated control mice (Supplemental Fig. 10A,B). We also evaluated *Stau1*, *Aif1* and *Gfap* mRNA levels in cerebellum by qPCR (Supplemental Fig. 10C-E). *Stau1* mRNA levels were ~40% reduced without activation of *Aif1*. However, a significant 15% increase of *Gfap* was observed for ASO-308 (p=0.005). Based on this we limited subsequent *in vivo* proof-of-concept studies to using only ASO-45.

Investigating the on-target effects of ASO-45

Alterations of motor phenotypes were not previously observed in mice null of *Stau1*, except for mildly reduced open field locomotor activity [10]. To confirm the observation, we performed open field behavioral testing using 6 month old *Stau1*$^{+/-}$, *Stau1*$^{-/-}$, and wild-type littermate mice by force plate actometry. No significant reduction on open field behavior determined as distance travelled was observed, or in percentage of time in chamber center 50%, and there were no sex differences (Supplemental Fig. 11A). To determine how ASO-45 modified open field behavior we treated WT mice that were 3 months of age with 300 µg ASO-45 for a duration of 3 wks. Again, we observed no significant reduction in open field

behavior, including distance travelled or time in chamber center 50%, and we observed no sex differences (Supplemental Fig. 11B). At the endpoint we evaluated *Stau1* mRNA levels in cerebellum by qPCR demonstrating significant *Stau1* reduction in ASO-45 treated mice (Supplemental Fig. 11C). We also performed a Pearson's correlation analysis of distance traveled to *Stau1* mRNA abundance, demonstrating no significant correlation (Supplemental Fig. 11D).

ASO-45 improves the molecular phenotypes in the spinal cord and motor cortex of *Prp*-TDP-43^{Q331K} mice

Spinal motor neuron pathology in TDP-43 mouse models is accompanied by reduced expression of ChAT, a motor neuron neurotransmitter, by NeuN, a pan-neuronal marker, together with increased GFAP, consistent with glial activation. These changes are also associated with impaired autophagy, including increased phospho-mTOR (p-mTOR), altered autophagy marker proteins, and activation of apoptosis. Previously, genetic reduction of *Stau1* in *Thy1*-hTDP-43 transgenic mice improved these molecular phenotypes, significantly normalizing mTOR, p-mTOR, pS6K, p62, LC3-II, cleaved CASP3 (cCASP3), and GFAP [6]. These findings provided the rationale for evaluating ASO-mediated STAU1 reduction as a therapeutic strategy TDP-43 proteinopathies.

We first evaluated ASO-45 dose response in *Prp*-TDP-43^{Q331K} mice. At 10 weeks, mice received 30, 100, or 300 µg ASO-45 by ICV injection and were analyzed 2 weeks later. Western blotting showed normalization of STAU1, GFAP, ChAT, cCASP3, mTOR, p62, and TDP-43 in spinal cord, with a dose-dependent reduction in hTDP-43 (Fig. 3A,B).

We next assessed whether ASO-45 could improve molecular phenotypes in motor cortex. *Prp-TDP-43^{Q331K}* mice were treated at 8 wks of age with 40 µg ASO-45 by ICV injection and analyzed after for 6 wks; this dose was selected based on the dose-ranging study. ASO-45 normalized STAU1, GFAP, NeuN and ChAT levels in motor cortex (Fig. 3C,D). In contrast, a non-targeting control ASO administered at 40 or 100 µg by ICV injection over the same 6 wk interval did not reduce STAU1 abundance in motor cortex (Supplementary Fig. 12).

ASO-45 restores TDP-43-dependent alternative splicing in the brain of *Prp-TDP-43^{Q331K}* mice.

We next determined whether ASO-45 has a similar effect on TDP-43-dependent splicing as *Stau1* genetic reduction in *Prp*-TDP-43^{Q331K} mice (Fig. 2E–G). *Prp*-TDP-43^{Q331K} mice and WT littermates were treated by ICV injection with 250 µg ASO-45 or PBS and analyzed 13 wks later. In cerebral hemispheres from the treated *Prp-TDP43^{Q331K}* mice, STAU1 abundance was more than twofold higher than in WT littermates and was reduced by more than 75% following ASO-45 treatment. ASO-45 treatment also significantly reduced human TDP-43^{Q331K} protein abundance (Fig. 3E,F). We then assessed alternative

splicing in Sort1, Kcnip2 and Ahi1 in cerebral hemispheres by RT-PCR. PBS-treated *Prp*-TDP-43^{Q331K} mice showed the expected aberrant splicing of all three transcripts, whereas ASO-45 significantly restored each event toward the WT pattern (Fig. 3G,H). Thus, sustained ASO-45 treatment corrects TDP-43-dependent splicing abnormalities in the brain, supporting a durable molecular benefit of STAU1 reduction in this model.

ASO-45 broadly attenuates the transcriptomic phenotype in the frontal cortex of *Prp*-TDP-43^{Q331K} mice.

To determine whether ASO-45 improves global transcriptomic abnormalities in *Prp*-TDP-43^{Q331K} mice, we performed RNA sequencing of frontal cortex from the same cohort analyzed for TDP-43-dependent splicing in Fig. 3E–H. WT and *Prp*-TDP-43^{Q331K} mice received PBS or 250 µg ASO-45 by ICV injection at 12 weeks of age and were analyzed at 26 weeks of age (n = 4 mice per group). Principal component analysis showed partial separation of samples by genotype and treatment condition, with some overlap among groups (Supplementary Fig. 13A). An UpSet plot summarizes DEG overlap across genotype and treatment comparisons and shows that the residual *Prp*-TDP-43^{Q331K}–associated DEG set after ASO-45 treatment was substantially smaller than the PBS-treated *Prp*-TDP-43^{Q331K} signature (Supplementary Fig. 13B). Differential-expression statistics, including $\log_2$ fold changes and adjusted P values for all genes and comparisons, are provided in Supplementary Data 1.

Heatmaps of the 40 most significant DEGs illustrate genotype-associated expression patterns and the genotype-dependent transcriptional response to ASO-45 (Fig. 4A,B). Volcano plots show predominantly downregulated genotype-associated DEGs and a predominantly upward transcriptional response to ASO-45 in *Prp*-TDP-43^{Q331K} mice (Fig. 4C,D). Residual genotype-associated expression differences persisted after treatment but were reduced relative to the PBS-treated comparison (Fig. 4E). ASO-45 altered only two genes in WT mice (Fig. 4F). Among the 866 DEGs identified between PBS-treated *Prp*-TDP-43^{Q331K} and WT mice, ASO-45 opposed the baseline expression difference for 732 genes (84.5%) and attenuated its magnitude for 785 genes (90.6%) (Fig. 4G,H). Median absolute genotype-associated $\log_2$ fold change decreased from 0.305 to 0.132 (56.6%), and 697 of 866 DEGs (80.5%) were no longer significantly different between ASO-45–treated *Prp*-TDP-43^{Q331K} and WT mice.

Gene set enrichment analysis using Hallmark and KEGG gene sets identified broad genotype- and treatment-associated pathway changes (Supplementary Fig. 13C,D; Supplementary Data 2). ASO-45 partially improved several *Prp*-TDP-43^{Q331K}–associated mitochondrial, metabolic, long-term-potentiation, axon-guidance, neurotrophin, MAPK, WNT, and synaptic programs. However, alterations in calcium-signaling, proteasome, spliceosome, and broader neuronal and chemical-synapse pathways persisted. Although ASO-45 treatment produced only two significant DEGs in WT mice, pathway-level analysis

identified enrichment of stress and inflammatory programs not significantly altered in PBS-treated *Prp*-TDP-43^{Q331K} mice. Together, these findings show that ASO-45 substantially attenuates, but does not fully normalize the cortical transcriptomic phenotype associated with TDP-43^{Q331K} expression.

ASO-45 improves molecular phenotypes in the spinal cord of *Thy1*-TDP-43$^{TG/+}$ mice

Having established efficacy in *Prp*-TDP-43^{Q331K} mice, we next evaluated ASO-45 in the independent *Thy1*-TDP-43 $^{Tg/+}$ model, which expresses human TDP-43 under control of the neuronal *Thy1* promoter. Twenty-four-wk old *Thy1*-TDP-43$^{Tg/+}$ mice were treated by ICV injection with ASO-45 and analyzed 2 wks later. We assessed STAU1, human TDP-43, ChAT, NeuN and GFAP in spinal cord lysates by western blotting.

ASO-45 significantly reduced spinal cord STAU1 in *Thy1*-TDP-43$^{TG/+}$ mice. Relative to WT mice, TG mice had reduced ChAT and NeuN and elevated GFAP; each was normalized or reduced toward WT levels by ASO-45. hTDP-43 was also reduced, and immunohistochemistry corroborated reduced motor-neuron TDP-43 and restored ChAT immunoreactivity (Fig. 5A–D).

ASO-45 improves survival and molecular phenotypes of *Thy1*-TDP-43$^{TG/TG}$ transgenic mice

To determine whether ASO-45-mediated reduction of STAU1 could improve survival of *Thy1*-TDP-43$^{TG/TG}$ mice, we treated neonates by ICV injection. In the first of two replicate studies, *Thy1*-TDP-43$^{Tg/+}$ breeders on a C57BL/6J background were used to generate homozygous mice. Pups were treated between postnatal days 1 and 3 with 10-30 µg ASO-45. Homozygous mice began to develop tremor at approximately postnatal day 12, and were monitored daily for 45 days for tremor and gait abnormalities using a neurological scoring system. Mice that were unable to right themselves withing 30 s were euthanized and assigned a neurological score of 4.

ASO-45 treatment significantly improved survival of *Thy1*-TDP-43$^{TG/TG}$ mice relative to vehicle treatment, extending lifespan by 15.7% (Fig. 5E). ASO-45 treatment also improved neurological scores at postnatal day18 (Fig. 5F).

We then analyzed whole-brain lysates from vehicle- and ASO-45-treated *Thy1*-TDP-43$^{TG/+}$ and *Thy1*-TDP-43$^{TG/TG}$ mice by western blotting (Fig. 5G,H). Relative to vehicle-treated WT mice, both *Thy1*-TDP-43$^{TG/+}$ and *Thy1*-TDP-43$^{TG/TG}$ mice showed elevated STAU1, GFAP and ATXN2 and cleaved CASP3, together with reduced NeuN and ChAT. ASO-45 treatment restored STAU1, GFAP, ATXN2, NeuN, and Chat levels toward WT values, with little effect on these proteins in WT mice. Although cleaved CASP3 was markedly elevated in *Thy1*-TDP-43$^{TG/TG}$ mice, ASO-45 reduced its abundance by approximately 23%, indicating partial improvement of this apoptotic marker. Complete sets of blots for WT, *Thy1*-TDP-43$^{TG/+}$ and *Thy1*-TDP-43$^{TG/TG}$ mice treated with PBS or ASO-45 are provided in Supplementary Fig. 14.

In a second survival study, we used *Thy1*-TDP-43$^{Tg/+}$ mice in the B6;SLJ background used by Becker *et al*. (2017) [1]. Mice were treated at postnatal day 3 with 30 µg ASO-45. As in the first study, ASO-45 significantly improved survival of *Thy1*-TDP-43$^{TG/TG}$ mice relative to vehicle treatment, extending lifespan of 9.5% (Supplemental Fig. 15A). Western blot analysis of spinal cord and cerebral hemispheres from *Thy1*-TDP-43$^{TG/TG}$ mice demonstrated significant reductions in STAU1 and human TDP-43 protein abundance following ASO-45 treatment (Supplementary Fig. 15B–D).

DISCUSSION

We used two complementary TDP-43 transgenic mouse models to assess whether STAU1 lowering modifies motor and survival outcomes, loss-of-function splicing abnormalities, and cytoplasmic autophagy-related pathology.

Development of disease modifying therapeutics

Disease-modifying therapeutics remain critically needed for neurodegenerative diseases. ASOs are clinically viable, as demonstrated by approved treatments for SOD1-ALS, spinal muscular atrophy (SMA) and Duchenne muscular dystrophy (DMD), and are being actively developed for other neurodegenerative disorders [11, 12, 13, 14]. Among such therapeutics is BIIB105 (ALSpire; ClinicalTrials.gov identifier NCT04494256), an antisense oligonucleotide targeting *ATXN2*. The preclinical version of BIIB105, differing in sequence, improved or normalized cerebellar molecular, motor, and electrophysiological phenotypes in ATXN2-Q127 mice [2]. In addition, reduction of *Atxn2* in in *Thy1*-TDP-43$^{TG/TG}$ ALS/FTD-like mice improved motor function and extended survival [1].

We recently discovered that STAU1, a component of ATXN2-associated RNA complexes, is overabundant across multiple neurodegenerative diseases, including patient-derived cell lines and rodent models [4, 5, 6]. Importantly, STAU1 levels were significantly elevated in spinal cord tissues from patients with *C9ORF72*-associated ALS and sporadic ALS, supporting its relevance across genetically defined and sporadic forms of ALS [5]. STAU1 overabundance perturbs mRNA metabolism, stress-granule dynamics, the UPR, and p53 signaling, whereas STAU1 knockdown normalizes these abnormalities. Together, these findings support STAU1 as a therapeutic target for neurodegenerative disease.

Studies supporting STAU1 therapeutics

STAU1 overabundance resulted in increased mTOR signaling by direct interaction between STAU1 and the 5'-UTR of the *MTOR* mRNA transcript resulting in its increased translation and altered autophagy [6]. Patient fibroblasts with overabundant STAU1 had hyperactivated mTOR and increased levels of autophagy marker proteins p62 and LC3-II. The same was true in the cerebella and spinal cords of ATXN2-Q127 mice and *Thy1*-TDP-43 mice [5]. Reducing STAU1 abundance leads to normalization of

autophagy markers and flux [5, 6]. STAU1 also modulates the unfolded protein response; its overexpression increases PERK, p-eIF2, and CHOP, whereas RNAi-mediated STAU1 reduction normalizes these mediators in TDP-43- and C9ORF72-mutant fibroblasts [15]. STAU1 overexpression in vivo impairs autophagy and activates glial and caspase pathways; in flies and mice, it worsens mutant TDP-43 and ATXN2 phenotypes [5]. STAU1 targeting may also be relevant to AD and related dementias: in cellular models, STAU1 promotes BACE1-dependent Aβ production and tau phosphorylation, both of which are reduced by lowering STAU1 abundance, and STAU1 is elevated in APP/PS1 mice [16, 17]. STAU1 may also intersect with RNA-surveillance pathways disrupted by TDP-43 dysfunction: Because STAU1 recruits UPF1 during STAU1-mediated mRNA decay (SMD) [18], STAU1 overabundance may contribute to disruption of the TDP-43–UPF1 RNA-regulatory axis recently described in ALS motor neurons [19].

Genetic interaction

Our initial genetic interaction studies supported STAU1 as a therapeutic target for NDD. Crossing SCA2 or TDP-43 transgenic mice with *Stau1* knockout mice, thereby lowering STAU1 abundance by 50%, improved molecular phenotypes in both models and improved behavioral phenotype in SCA2 mice [4, 6]. Here we extended these studies by crossing *Prp*-TDP-43^{Q331K} mice with *Stau1*$^{+/-}$ mice. *Prp*-TDP-43^{Q331K} mice exhibited significant behavioral and motor deficits, including impaired rotarod performance, grip strength, hind-limb clasping, and open-field activity, relative to wild-type and *Stau1*$^{+/-}$ littermates. In contrast, partial *Stau1* reduction significantly ameliorated these measures. *Stau1* haploinsufficiency in *Prp*-TDP-43^{Q331K} mice also improved TDP-43-dependent splicing of *Sort1*, *Kcnip2*, and *Ahi1*, transcripts previously shown to be aberrantly spliced in association with TDP-43^{Q331K} expression. Moreover, transcriptomic analysis identified numerous differentially expressed genes, predominantly reduced in *Prp*-TDP-43^{Q331K} mice, whose expression changes were generally attenuated or reversed by *Stau1* haploinsufficiency. Together, these independent genetic interaction studies identify STAU1 as a modifier of TDP-43-associated pathology and support STAU1 reduction as a therapeutic strategy for TDP-43 proteinopathies, including ALS and FTD.

Selection and in vivo engagement of ASO-45

The targeted ASO screen identified MOE gapmer ASOs that reduced *STAU1* expression *in vitro* and *in vivo*. To limit predicted RNA-dependent off-target effects, candidate ASOs were assessed for sequence identity to CNS-expressed genes by alignment to the human genome, and ASOs with complementarity to *STAU2*, which is also overabundant in neurodegenerative disease [20], were excluded. The most efficacious ASOs targeted all Ensembl-annotated *STAU1* isoforms and were validated in patient fibroblasts and BAC-STAU1 mice, yielding a small set of potent candidates. ASO-45 had only one predicted human off-target and no predicted mouse off-targets by alignment to the mouse genome. Consistent with limited off-

target activity, RNA sequencing identified only two significantly altered genes in ASO-45–treated WT mice relative to PBS-treated WT mice. WT mice treated with ASO-45 showed no locomotor or center-crossing differences relative to controls (Fig. 1D,E; Supplementary Fig. 11). This was also confirmed in *Stau1*$^{+/-}$ nor *Stau1*$^{-/-}$ mice as neither line showed reduced locomotion. Subtle effects on functional synapses reported by others, however, were not examined [10]. Together, these data support robust target engagement by ASO-45 with limited predicted RNA-dependent off-target activity and no evident adverse behavioral consequence of *Stau1* on-target reduction.

Effect of ASO-45 on TDP-43–associated phenotypes

TDP-43 proteinopathy is characterized by cytoplasmic mislocalization and nuclear loss of function. In *Prp*-TDP-43^{Q331K} mice, ASO-45 normalized elevated STAU1 and improved spinal-cord markers of gliosis, neuronal health, apoptosis, and autophagy; GFAP, NeuN, and ChAT were also restored in motor cortex. Similar molecular and histological effects occurred in *Thy1*-TDP-43$^{TG/+}$ mice, including reduced motor-neuron TDP-43 (Figs. 3 and 5). Across the tested models, both genetic *Stau1* reduction and ASO-45 treatment reduced GFAP toward wild-type levels, consistent with attenuation of astroglial activation, a process implicated in ALS disease progression.

A major aspect of TDP-43 pathology is a splicopathy, characterized by missplicing of subsets of RNA and cryptic exon inclusion. We identified disease-associated alternative splicing of *Sort1*, two *Kcnip2* variants, and *Ahi1* in *Prp*-TDP-43^{Q331K} and BAC-STAU1 mice (Supplementary Fig. 3), although we did not detect the cryptic exon inclusion in *Ap2b3* and *Camk1g* reported elsewhere [21], These events are associated with reduced nuclear TDP-43 activity [9], and ASO-45 significantly reversed all three abnormalities in *Prp*-TDP-43^{Q331K} mice (Fig. 3).

These molecular and cellular effects were accompanied by functional benefit in *Thy1*-TDP-43$^{TG/TG}$ mice. ASO-45 improved neurological scores and extended survival by 15.7% in C57BL/6J mice, with normalization of GFAP, ATXN2, NeuN, ChAT, and cCASP3 in cerebral hemispheres (Fig. 5). In an independent B6;SJL cohort, selected for a more pronounced ALS-like hindlimb phenotype [1], ASO-45 again significantly extended survival (9.5%) and improved molecular disease markers in spinal cord and brain (Supplementary Fig. 15).

Potential limitations

Although ASO-45 produced robust molecular and phenotypic effects in mouse models, the long-term consequences of sustained STAU1 reduction remain undefined. These models also do not capture the full clinical and pathological heterogeneity of human ALS and related disorders. Although bioinformatic screening and *in vivo* analyses suggested limited predicted off-target effects, transcriptome-wide studies

will be needed to further define RNA-dependent off-target activity of STAU1-directed ASOs. Whereas genetic *Stau1* haploinsufficiency reduces STAU1 in all cell types, ASO uptake in the CNS may favor neurons over glia. The relative contributions of neuronal and glial STAU1 lowering to the observed therapeutic effects therefore remain unresolved. However, the behavioral, splicing, and transcriptomic improvements produced by genetic *Stau1* haploinsufficiency independently support STAU1 as a modifier of TDP-43-associated pathology.

Conclusions

STAU1 is overabundant in models relevant to SCA2, ALS, AD, and HD. Partial STAU1 reduction improves disease phenotypes in mouse models of SCA2 and ALS and reduces AD-relevant amyloidogenic and tau-phosphorylation. Here, lowering STAU1 in rodent models modified molecular, cellular, behavioral, and survival phenotypes and restored TDP-43-dependent splicing, consistent with improved nuclear function. Unlike approaches directed at mutant proteins or repeat expansions, STAU1 targeting leverages its role at the intersection of stress-granule dynamics, mTOR-dependent autophagy, and RNA processing. Overabundance of STAU1 in spinal cords of individuals with sporadic ALS suggest STAU1 as a potential therapeutic target for the majority of ALS patients. Together, these findings support STAU1-directed ASO therapy as a mechanistically distinct therapeutic strategy for TDP-43-associated neurodegeneration.

MATERIALS AND METHODS

Study design

This study was designed to evaluate antisense oligonucleotides (ASOs) targeting STAU1 as a therapeutic strategy for TDP-43–related neurodegeneration. Experiments were performed in cultured cells and in mouse models to assess ASO efficacy. Initial ASO screening and dose–response analyses were conducted in HEK-293 cells and patient-derived SCA2 fibroblasts, followed by *in vivo* evaluation after intracerebroventricular (ICV) delivery in mouse models expressing human TDP-43 or hSTAU1.

Molecular outcomes were assessed using qPCR, RT-PCR, western blotting, and immunohistochemistry, and behavioral and survival outcomes were evaluated in mice. Experiments were repeated independently as indicated in figure legends. Animals were assigned to treatment groups as described below, and investigators performing outcome assessments were blinded to genotype or treatment where indicated. Statistical tests are described in the Statistical Analysis section.

Antisense oligonucleotides (ASOs)

ASOs used in this study were 20mer 5-10-5 2'-*O*-methoxyethyl (MOE) gapmers, phosphorothioated at all positions. All cytosine positions were methylated. ASOs were produced and purified by Integrated DNA Technologies (IDT). Preparations included desalting for *in vitro* work or HPLC purification and dialysis to remove chromatography solvent for *in vivo* work.

Cell culture

HEK-293 or SCA2 patient-derived skin fibroblasts (SCA2-500-1), expressing ATXN2 Q22/Q45, were cultured and maintained in Dulbecco's modified Eagle's medium (DMEM, high glucose, ThermoFisher #11965118) supplemented with 10% fetal bovine serum, and 1x penicillin and streptomycin. The SCA2-500-1 patient fibroblasts were previously collected by us, with written consent, and the studies were approved by the Institutional Review Board at the University of Utah. HEK-293 cells were transfected with ASOs using Lipofectamine, while SCA2-500-1 cells were transfected with Lipofectamine 3000, according to manufacturer's protocol (ThermoFisher). The cells were harvested at 48 or 72 hrs post-transfection for analyses.

Cell Line Authentication

In order to adhere with the National Institutes of Health (NIH) guideline on scientific rigor in conducting biomedical research (NOT-OD-15-103) on the use of biological and/or chemical resources, we authenticated both the HEK-293 and SCA2-500-1 cell lines by STR analysis on 24 loci, including amelogenin for sex identification. The kit used for this was the GenePrint 24 system (Promega).

Mice

B6.Cg-Tg(Prnp-TARDBP*Q331K)103Dwc/J mice (*Prp*-TDP43^{Q331K} mice) (Jackson Laboratories 017933) [9] were maintained in the C57BL/6J background. The *Stau1*$^{tm1Apa(-/-)}$ (*Stau1*$^{-/-}$) mouse [10] was a generous gift from Prof. Michael A. Kiebler, Ludwig Maximilian University of Munich, Germany, and maintained in a C57BL/6J background. B6;SJL-Tg(Thy1-TARDBP)4Singh/J mice (*Thy1*-TDP-43 mice) (Jackson Laboratories 012836) [22] were maintained in two different ways, including in the B6;SJL as previously described [6] and in C57BL/6J background after backcrossing. For survival studies using *Thy1*-TARDBP mice, hemizygous mice were crossed to produce the homozygous genotype; genotyping was conducted as previously described [6]. The BAC-STAU1 mouse model is previously described and maintained on a B6D2 mixed background by backcrossing to B6D2F1J no less than every 4 generations [8]. Mice were maintained in a temperature and humidity-controlled environment on a 12h light/dark cycle with light onset at 6:00 AM. All studies and procedures were approved by an Institutional Animal Care and Use Committee (IACUC) at the University of Utah, SLC, UT.

ICV ASO Injections

ASOs were delivered to adult mice by ICV injection using a Hamilton 26s gauge needle (Hamilton # 7758-02). Injections volumes were 10 µl of ASO diluted in phosphate buffered saline (PBS). Control mice received the same volume of normal saline. Injections were made under anesthesia with a mixture of oxygen and isoflurane, using a Stoelting stereotaxic frame. Anesthesia was initiated using 3% isoflurane for 5 min and the isoflurane mixture was lowered to 2% during injections. Stereotaxic bregma coordinates were -0.46 mm anteroposterior, -1.0 mm lateral (right side); -2.5 mm dorsoventral. Needles were removed 4 min after ASO delivery. Mice were maintained on a 39°C isothermal pad while anesthetized and during recovery. Neonate mice were treated by ICV injections following [23] using a Hamilton 32 gauge needle (Hamilton # 7803-04). Mice were cryoanesthesized and treated ICV in either of two ways, including single treatments to the right lateral ventrical using a volume of 3 µl, or bilateral treatments to both the left and right ventricals using a volume of 2 µl in each ventricle.

Quantitative PCR (qPCR)

For medium throughput assays performed in ASO screens and IC50 studies we used the Cells-to-Ct assays (ThermoFisher). These assays were combined with Taqman qPCR kits for human *STAU1* (ThermoFisher Hs00244999_m1) and human *ACTB* (Thermofisher Hs01060665_g1). For other qPCRs, standard SYBR Green assays were performed as follows: Total RNA was extracted from cultured cells, cerebellar tissues or spinal cord tissues using the RNeasyMini Kit (Qiagen Inc., USA) according to the manufacturer's protocol. DNAse I treated RNAs were used to synthesize cDNAs using the ProtoScript cDNA First Strand cDNA Synthesis Kit (New England Biolabs Inc., USA). Primers for RT-PCR were designed to prevent amplification from genomic DNA (annealing sites in different exons or across intron-exon boundaries). Quantitative RT-PCR was performed in Bio-Rad CFX96 (Bio-Rad Inc., USA) with the Power SYBR Green PCRMasterMix (Applied Biosystems Inc, USA). PCR reaction mixtures contained SYBR Green PCRMasterMix and 0.5 pmol primers and PCR amplification was carried out for 45 cycles: denaturation at 95 °C for 10 sec, annealing at 60 °C for 10 sec and extension at 72 °C for 40 sec. The threshold cycle for each sample was chosen from the linear range and converted to a starting quantity by interpolation from a standard curve run on the same plate for each set of primers. Gene expression levels were normalized to the *Actin* mRNA levels. Four human transcripts, primers included STAU1-F 5'-TCCTTGGTTTCAAAGTCCCG-3' and STAU1-R 5'-ATTTTCATCCCCAGAGCCAG-3'; ACTB-F: 5'-GAAAATCTGGCACCACACCT-3' and ACTB-R: 5'-TAGCACAGCCTGGATAGCAA-3'. For mouse transcripts, primers included Stau1-F: 5'-AGTACATGCTCCTTACAGAACG-3' and Stau1-R: 5'-TGATGCCCAACCTTTACCTG-3'; Aif1-A1: 5'-CTGGAGGGGATCAACAAGCAATTC-3' and Aif-B2: 5'-CCAGCATTCGCTTCAAGGACATAA-3'; Gfap-for: 5'-CGGAGACGCATCACCTGTG-3' and Gfap-rev: 5'-AGGGAGTGGAGGAGTCATTCG-3'; Actb-F: 5'-CGTCGACAACGGCTCCGGCATG-3'

and Actb-R: 5'-GGGCCTCGTCACCCACATAGGAG-3'; Mouse Actb-F: 5'-CGTCGACAACGGCTCCGGCATG-3' and Actb-R: 5'-GGGCCTCGTCACCCACATAGGAG-3'.

Western blot analyses

Protein extracts were prepared by homogenization of mouse cerebella in extraction buffer (25 mM Tris-HCl pH 7.6, 300 mM NaCl, 0.5% Nonidet P-40, 2 mM EDTA, 2 mM MgCl2, 0.5 M urea and protease inhibitors; Sigma; cat# P-8340) followed by centrifugation at 4°C for 20 min at 16,100 × g. Protein extracts were resolved by SDS-PAGE and transferred to Hybond P membranes (Amersham Bioscience Inc., USA). After blocking with 5% skim milk in 0.1% Tween 20/PBS, the membranes were incubated with primary antibodies in 5% skim milk in 0.1% Tween 20/PBS for 2 hrs at room temperature or overnight at 4°C. After washing in 0.1% Tween 20/PBS, the membranes were incubated with the corresponding secondary antibodies conjugated with HRP in 5% skim milk in 0.1% Tween 20/PBS for 2 hrs at room temperature and washed again. Signals were detected by using the Immobilon Western Chemiluminescent HRP Substrate (Millipore Inc., USA; cat# WBKLSO100) according to the manufacturer's protocol, and detected using a ChemiDoc System (Bio-Rad). The intensity of proteins was determined using the ChemiDoc software and proteins were quantitated as a ratio to β-Actin.

Antibodies

Antibodies included the following: rabbit polyclonal anti-Staufen antibody (Novus Biologicals, NBP1-33202); rabbit polyclonal anti-mTOR antibody (Cell Signaling Technology, 2972); rabbit polyclonal anti-Phospho-mTOR (Ser2448) [(1:3000), Cell Signaling Technology, 2971]; rabbit polyclonal anti-SQSTM1/p62 antibody (Cell Signaling Technology, 5114); rabbit polyclonal anti-LC3B antibody (Novus Biologicals, NB100-2220); mouse monoclonal anti-TDP-43 (human specific) antibody (Proteintech 60019-2-Ig); rabbit polyclonal human/mouse anti-TDP-43 antibody (Proteintech 10782-2-AP); mouse monoclonal anti-Calbindin-D-28K antibody [(1:5000), Sigma-Aldrich, C9848]; rabbit polyclonal anti-RGS8 antibody [(1:5000), Novus Biologicals, NBP2-20153]; mouse monoclonal anti-PCP2 antibody (F-3) [(1:3000), Santa Cruz, sc-137064]; rabbit polyclonal anti-PCP4 antibody [(1:5000), Abcam, ab197377]; Phospho-p70 S6 Kinase (Thr389) antibody [(1:3000), Cell Signaling, Cat# 9205]; GFAP (GA5) mouse mAb [(1:7000), Cell signaling, Cat #3670]; ChAT (E4F9G) Rabbit mAb [(1:5000), Cell Signaling, Cat# 27269]; NeuN (D4G4O) XP® Rabbit mAb [(1:5000), Cell Signaling, Cat# 24307]; GAPDH (14C10) rabbit mAb [(1:7,000), Cell Signaling, Cat# 2118]; Cleaved Caspase-3 (Asp175) (5A1E) rabbit mAb [(1:3000), Cell Signaling, Cat #9664]; Anti-FAM107B antibody [(1:5,000) Abcam, ab175148); and mouse monoclonal anti-β-Actin−peroxidase antibody (clone AC-15) (Sigma-Aldrich, A3854). Secondary antibodies included peroxidase-conjugated horse anti-mouse IgG (Vector Laboratories, PI-2000) and peroxidase AffiniPure goat anti-rabbit IgG (Jackson ImmunoResearch Laboratories, 111-035-144).

Immunofluorescent and immunohistochemical staining

Immunofluorescent labeling: Sections were deparaffinized and rehydrated, and antigen retrieval was performed by microwave in Citrate-Based (Vector Laboratories (VWR) H-3300-250). Sections were blocked and permeabilized in 10% goat serum with 0.1% Triton X-100 for 1 h at room temperature. The primary antibody was mouse monoclonal anti-TDP-43 (human-specific) (Proteintech 60019-2-Ig, used at a 1:3000 dilution). The secondary antibody was goat anti-mouse IgG (H+L) highly cross-adsorbed secondary antibody (Thermo Fisher Scientific, Alexa Fluor™ Plus 647- A32728, used at 1:1000). Nuclei were counterstained with 4′,6-diamidino-2-phenylindole (DAPI; Thermo Fisher Scientific D1306) at 1 µg/mL. Slides were mounted using ProLong™ gold antifade mountant (Thermo Fisher Scientific P36934). Confocal images were acquired using a Leica SP8 confocal microscope equipped with a white-light laser and a 20× objective.

Immunohistochemical staining: Spinal cords were removed, and fixed in 4% paraformaldehyde/PBS and cryoprotected stepwise in 10, 20, then 30% sucrose/PBS. Tissues were embedded in OCT and sectioned (20 µm). Sections were labeled with human-specific anti-TDP-43 antibody (see above) or ChAT (H-95) polyclonal antibody (Santa Cruz Biotechnology sc-20672) as previously described [4], and brightfield images were produced using an Olympus BX53 inverted microscope with a 40x objective. Regions of interest (ROIs) were selected manually around ventral horn MNs with clear evidence of a nucleolus. Staining intensity in ROIs was determined using NIH Elements software package, and reported as intensity per motor neuron.

Open field behavioral phenotype testing

Genetic interaction study: Mice were tested in a custom-built 50 × 50 cm gray open-field arena under dim, full-spectrum LED lighting that did not heat the arena. Head and tail positions were tracked for 10 min using an overhead camera, and open-field metrics were calculated using ANY-maze video-tracking software (Stoelting). Animals were habituated in the testing room for at least 60 min before testing.

On-target open-field behavioral testing: Open-field behavior was assessed using a force plate actometer [24]. The actometer hardware and MATLAB-based analysis pipeline were as previously described [25, 26]. Center-of-mass position was sampled at 1,000 Hz and recorded using LabVIEW (National Instruments). The analysis applied a 1-s running-average filter to center-of-mass data and calculated total distance traveled during each recording. Animals were habituated in the testing room for at least 30 min before testing. The room was well isolated from external noise and maintained under dim, uniform lighting, as measured with a luxometer. Recordings were made for either 10 or 30 min and total distance traveled was calculated.

Reverse transcription PCR (RT-PCR)

Mice were deeply anesthetized with isoflurane. Spinal cords and brain hemispheres were dissected and rapidly frozen. Tissues were stored at −80 °C until further processing. Total RNA was extracted from mouse tissues using the RNeasy mini-kit according to the manufacturer's protocol (Qiagen, USA). RNA integrity numbers (RINs) were determined using the Agilent 2200 TapeStation and ranged from 8.2 to 9.3. DNase I-treated RNA samples were used to synthesize cDNA with the High-Capacity cDNA Reverse Transcription Kit (Thermo Fisher Scientific; catalog no. 4368814). To study alternative RNA splicing, RT-PCR reactions were performed using 150 ng of cDNA derived from total RNA, with 35 amplification cycles. PCR primers included the following: Sort1-exon-17F (5'-CAAATGCCAAGGTGGGATGAA-3') & Sort1-exon-19R (5'-TGACAAGCATCAGTCCCACGAT-3'), Kcnip2-exon-1F (5'-GAGCGGGGCGCCGGGGGCCATGCG-3') & Kcnip2-exon-4R (5'-AACTTGGTTTGTTCCTGGAGTTG-3'), and Ahi1-exon-16F (5'-GATTCAACTTGTGAAACAGAG-3') & Ahi1-exon-18R (5'-GTGGTGGCGAAGTCATTGAGAG-3'). In all cases, the PCR products were cloned and verified by sequencing. Band intensities were measured using the Fiji/ImageJ software package (https://imagej.net/Fiji) after image inversion. Splicing was quantified as the ratio of exon inclusion (Incl) to exon exclusion (Excl), or *vice versa*, as indicated in figures. RT-PCR was also performed to evaluate the expression of human TDP-43 (*TARDBP*) and human *STAU1*, relative to mouse *Actb*, using cDNA derived from total RNA with 35 cycles. PCR primers used included the following: TDP43-EX5F (5'-TCTCTCAGTACGGGGATGTGA-3') & TDP43-MUT331R (5'-CCATCATACCCCAACTGCTCTT3'), STAU1-F796 (5'-GTGGAACTTTCTGTGGGAGG-3') & STAU1-R1427 (5'-ATTTTCATCCCCAGAGCCAG-3'), mActin-F344 (5'-ACCTTCTACAATGAGCTGCG-3') & mActin-R490 (5'-CTGGATGGCTACGTACATGG-3').

Transcriptomic analysis

RNA isolation and sequencing: Sixteen 26-week-old mice were analyzed, with four biological replicates per genotype–treatment group and equal representation of males and females. Total RNA was extracted from frontal cortex using the RNeasy Mini Kit (Qiagen). All samples had RNA integrity numbers greater than 9.0. Stranded UMI-based 3′ mRNA sequencing was performed by Plasmidsaurus on an Illumina NovaSeq X Plus RNA-sequencing data processing: Reads were aligned to the *Mus musculus* GRCm39 reference genome from Ensembl (GCA_000001635.9) and deduplicated using UMIs. Gene-level counts were generated from reads assigned to exons and 3′ untranslated regions using Ensembl gene identifiers. Processed counts were provided to the Huntsman Cancer Institute Bioinformatics Core for downstream analysis.

Differential expression was analyzed using DESeq2 with the model ~ status + sex, where status represented the four genotype–treatment groups. Genes with a Benjamini–Hochberg-adjusted P value below 0.05 were considered differentially expressed. No log2 fold-change cutoff was applied, independent filtering was disabled, and fold-change estimates were shrunk using the normal estimator. Genotype-dependent treatment responses were evaluated using the model ~ sex + genotype x treatment. Regularized-logarithm-transformed counts were used for principal-component analysis and heatmaps, and gene-set overlap was visualized using UpSetR.

Pre-ranked gene-set enrichment analysis was performed using fgsea. Genes were ranked by shrunken log2 fold change without significance or effect-size filtering. Shrunken $\log_2$ fold-change estimates were used for fold-change comparisons and gene-level improvement analyses. Hallmark and KEGG gene sets were obtained from the Molecular Signatures Database through hciRdata in August 2026. Gene sets with an adjusted P value below 0.10 were considered significant.

Transcriptomic scatterplot analyses were restricted to the 866 genes differentially expressed in TG-PBS versus WT-PBS (adjusted $P < 0.05$). For each baseline TG-associated differentially expressed gene, the ASO-45 response in transgenic mice was defined as the log2 fold change for TG-ASO versus TG-PBS. Responses with a direction opposite to the baseline TG-associated log2 fold change were classified as opposing, whereas those with the same direction were classified as concordant. Opposing responses with adjusted $P < 0.05$ in the TG-ASO versus TG-PBS comparison were designated significant opposing responses.

To assess residual TG-associated expression differences after treatment, the residual TG-ASO versus WT-ASO log2 fold change was compared with the baseline TG-PBS versus WT-PBS log2 fold change. A gene was classified as attenuated when the absolute residual log2 fold change was smaller than the absolute baseline TG-associated log2 fold change. Percentage reduction was calculated as $100 \times [|\text{untreated difference}| - |\text{residual difference}|]/|\text{untreated difference}|$. Genes with an adjusted P value ≥ 0.05 in the TG-ASO versus WT-ASO comparison were classified as no longer significantly different from WT after treatment. Figures were generated in R using the readxl, dplyr, and ggplot2 packages; code is available at [insert Github/DOI].

Survival Analysis

Homozygous *Thy1*-TDP-43 transgenic mice begin to show signs of illness in the form of tremor usually in the second week of life. Once tremor was evident for any mice within a cohort, all mice were monitored daily. A prespecified humane endpoint was defined as the inability to maintain an upright posture when placed in the standing position and failure to right within 30 seconds. Mice were assessed

longitudinally using a semi-quantitative neurological score, ranging from 1 to 4. A score of 1 was assigned at the first observable tremor. A score of 2 was assigned upon the onset of gait impairment following tremor. A score of 3 reflected clear progression of tremor and motor disability. A score of 4 was assigned when mice were unable to right themselves within 30 seconds, meeting the humane endpoint criteria and prompting euthanized. Death as an endpoint was not used. Time to euthanasia was recorded for statistical analysis. Determination of euthanasia timing was made by a technician blinded to genotype.

Statistical Analysis

Statistical differences between selected groups evaluated by qPCR, western blotting, and the electrophysiological data were also evaluated using analysis of variance (ANOVA) tests followed by post-hoc tests of significance (Tukey's or Bonferroni's tests for multiple comparison, as indicated). Student's *t*-tests were unpaired and two-tailed. All tests were performed using the GraphPad Prism 10 software package except for tests of on target open field behavior data that were performed in MATLAB. Survival analyses were performed in GraphPad Prism 10 using the log-rank (Mantel-Cox) test, with hazard ratio determined by the log-rank text. No data points were excluded as outliers.

References

1. Becker, L. A.*, et al.* Therapeutic reduction of ataxin-2 extends lifespan and reduces pathology in TDP-43 mice. *Nature* **544**, 367-371 https://doi.org/10.1038/nature22038 (2017).
2. Scoles, D. R.*, et al.* Antisense oligonucleotide therapy for spinocerebellar ataxia type 2. *Nature* **544**, 362-366 https://doi.org/10.1038/nature22044 (2017).
3. Li, X. & Bedlack, R. Evaluating emerging drugs in phase II & III for the treatment of amyotrophic lateral sclerosis. *Expert Opin Emerg Drugs* **29**, 93-102 https://doi.org/10.1080/14728214.2024.2333420 (2024).
4. Paul, S., Dansithong, W., Figueroa, K. P., Scoles, D. R. & Pulst, S. M. Staufen1 links RNA stress granules and autophagy in a model of neurodegeneration. *Nat Commun* **9**, 3648 https://doi.org/10.1038/s41467-018-06041-3 (2018).
5. Paul, S.*, et al.* Staufen1 in Human Neurodegeneration. *Ann Neurol* **89**, 1114-1128 https://doi.org/10.1002/ana.26069 (2021).
6. Paul, S.*, et al.* Staufen impairs autophagy in neurodegeneration. *Ann Neurol* **93**, 398-416 https://doi.org/10.1002/ana.26515 (2023).
7. Zhao, R.*, et al.* Excessive STAU1 condensate drives mTOR translation and autophagy dysfunction in neurodegeneration. *The Journal of cell biology* **223**, https://doi.org/10.1083/jcb.202311127 (2024).

8. Pulst, S. M.*, et al.* A human Staufen1 BAC transgenic mouse exhibits abnormal autophagy and neurodegeneration across the central nervous system. *Cell Death Dis* **17**, https://doi.org/10.1038/s41419-026-08830-x (2026).
9. Arnold, E. S.*, et al.* ALS-linked TDP-43 mutations produce aberrant RNA splicing and adult-onset motor neuron disease without aggregation or loss of nuclear TDP-43. *Proc Natl Acad Sci U S A* **110**, E736-745 https://doi.org/10.1073/pnas.1222809110 (2013).
10. Vessey, J. P.*, et al.* A loss of function allele for murine Staufen1 leads to impairment of dendritic Staufen1-RNP delivery and dendritic spine morphogenesis. *Proc Natl Acad Sci U S A* **105**, 16374-16379 https://doi.org/10.1073/pnas.0804583105 (2008).
11. Bennett, C. F., Krainer, A. R. & Cleveland, D. W. Antisense Oligonucleotide Therapies for Neurodegenerative Diseases. *Annu Rev Neurosci* **42**, 385-406 https://doi.org/10.1146/annurev-neuro-070918-050501 (2019).
12. Iftikhar, M., Frey, J., Shohan, M. J., Malek, S. & Mousa, S. A. Current and emerging therapies for Duchenne muscular dystrophy and spinal muscular atrophy. *Pharmacol Ther* **220**, 107719 https://doi.org/10.1016/j.pharmthera.2020.107719 (2021).
13. Torres-Masjoan, L., Aguti, S., Zhou, H. & Muntoni, F. Clinical applications of exon-skipping antisense oligonucleotides in neuromuscular diseases. *Mol Ther* **33**, 2689-2704 https://doi.org/10.1016/j.ymthe.2025.04.038 (2025).
14. Ravits, J., Ferrey, D., Gundogdu, B., Qayoumi, W. & Zale, C. Amyotrophic Lateral Sclerosis: A Review. *JAMA* **335**, 1970-1982 https://doi.org/10.1001/jama.2026.6385 (2026).
15. Gandelman, M.*, et al.* Staufen 1 amplifies proapoptotic activation of the unfolded protein response. *Cell Death Differ* **27**, 2942-2951 https://doi.org/10.1038/s41418-020-0553-9 (2020).
16. Silva-Llanes, I., Baceiredo-Macho, P. & Lastres-Becker, I. Analysis of the involvement of RNA-binding proteins in TAU-dependent neurodegeneration. *Neurobiol Dis* **226**, 107454 https://doi.org/10.1016/j.nbd.2026.107454 (2026).
17. Li, C. L.*, et al.* STAU1 exhibits a dual function by promoting amyloidogenesis and tau phosphorylation in cultured cells. *Exp Neurol* **377**, 114805 https://doi.org/10.1016/j.expneurol.2024.114805 (2024).
18. Kim, Y. K., Furic, L., Desgroseillers, L. & Maquat, L. E. Mammalian Staufen1 recruits Upf1 to specific mRNA 3'UTRs so as to elicit mRNA decay. *Cell* **120**, 195-208 https://doi.org/10.1016/j.cell.2004.11.050 (2005).
19. Alessandrini, F.*, et al.* TDP-43 dysfunction compromises UPF1-dependent mRNA metabolism in ALS. *Neuron* **114**, 640-660 e610 https://doi.org/10.1016/j.neuron.2025.11.001 (2026).

20. Paul, S.*, et al.* Staufen2 dysregulation in neurodegenerative disease. *J Biol Chem* **301**, 108316 https://doi.org/10.1016/j.jbc.2025.108316 (2025).
21. Jeong, Y. H.*, et al.* Tdp-43 cryptic exons are highly variable between cell types. *Mol Neurodegener* **12**, 13 https://doi.org/10.1186/s13024-016-0144-x (2017).
22. Wils, H.*, et al.* TDP-43 transgenic mice develop spastic paralysis and neuronal inclusions characteristic of ALS and frontotemporal lobar degeneration. *Proc Natl Acad Sci U S A* **107**, 3858-3863 https://doi.org/10.1073/pnas.0912417107 (2010).
23. Kim, J. Y.*, et al.* Viral transduction of the neonatal brain delivers controllable genetic mosaicism for visualising and manipulating neuronal circuits in vivo. *Eur J Neurosci* **37**, 1203-1220 https://doi.org/10.1111/ejn.12126 (2013).
24. Fowler, S. C.*, et al.* A force-plate actometer for quantitating rodent behaviors: illustrative data on locomotion, rotation, spatial patterning, stereotypies, and tremor. *J Neurosci Methods* **107**, 107-124 https://doi.org/10.1016/s0165-0270(01)00359-4 (2001).
25. Anderson, C. J., Figueroa, K. P., Dorval, A. D. & Pulst, S. M. Deep cerebellar stimulation reduces ataxic motor symptoms in the shaker rat. *Ann Neurol* **85**, 681-690 https://doi.org/10.1002/ana.25464 (2019).
26. Figueroa, K. P.*, et al.* Slc9a6 mutation causes Purkinje cell loss and ataxia in the shaker rat. *Hum Mol Genet* **32**, 1647-1659 https://doi.org/10.1093/hmg/ddad004 (2023).

Acknowledgements

We thank Justine Sundrud, Erika Aoyama, Gentrie Maag, and Alexandar Price for contributing to work in this study. We also extend our gratitude to Siew Peng Ho, William Murray, and Simon MazzaLunn who served as Harrington Discovery Institute (HDI) advisors to DRS in association with support by the HDI Rare Disease Scholarship for development of *STAU1* ASOs. We thank the Huntsman Cancer Institute High-Throughput Genomics and Cancer Bioinformatics Shared Resource, supported by the NCI Cancer Center Support Grant P30CA042014, for RNA quality control, library preparation, sequencing, and primary data processing; the ARUP Research Histology Core, University of Utah, for paraffin processing,

sectioning, and slide preparation; and the University of Utah Cell Imaging Core for access to the Leica SP8 confocal microscope. We thank the University of Utah Health Sciences Machine Shop for assistance constructing the custom open-field arena. This work was supported in part by the Dale L. Rindlisbacher Endowed Chair in Neurodegeneration (SMP) and the Dr. John P. Punke Endowed Chair in Neurology (DRS).

Funding:

Harrington Discovery Institute Rare Disease Scholar Award (DRS)
National Institutes of Health (NIH) grant R01NS097903 (DRS)
National Institutes of Health (NIH) grant R01NS137233 (DRS)
National Institutes of Health (NIH) grant R21NS128630 (DRS, MG)
National Institutes of Health (NIH) grant R21NS127028 (DRS)
National Institutes of Health (NIH) grant R56NS033123 (SMP)
National Institutes of Health (NIH) grant R37NS033123 (SMP)
National Institutes of Health (NIH) grant R35NS127253 (SMP)
National Institutes of Health (NIH) grant R61/R33NS124965 (DRS, SMP)
U.S. Department of Defense (DoD/ALSRP) grant AL240089 (Eugene Yeo; subaward to SMP, DRS).

Author Contributions:

Conceptualization: SMP, DRS
Methodology: DRS, SMP, SP, MG, WD, PH, KPF, CJA
Investigation: DRS, SP, MG, KPF, WD, JL, PH, CJA
Visualization: DRS, SP, MG, PH
Funding acquisition: DRS, SMP, MG
Project administration: DRS, KPF
Supervision: DRS, SMP
Writing – original draft: DRS, SMP
Writing – review & editing: DRS, SMP, SP, KPF, MG

Competing interests:

D.R.S., S.M.P. and S.P. are inventors on a patent application related to this work ("Staufen1 agents and associated methods," patent no. 11723912). All other authors declare that they have no competing interests.

Data and materials availability:

All data not provided in the supplementary materials are available upon request. All materials generated in this study including ASOs are commercially available or will be supplied upon request.

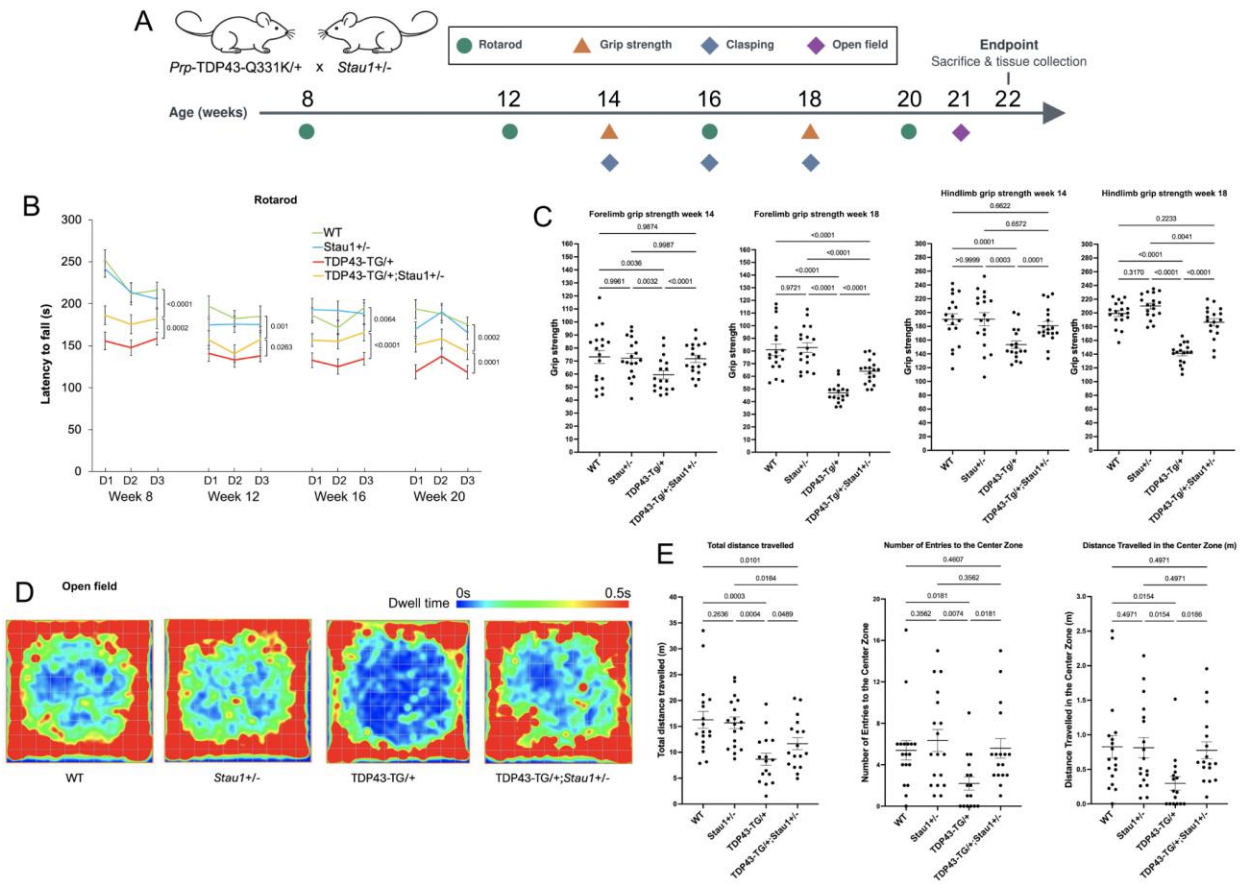


Fig. 1. Genetic reduction of *Stau1* in *Prp*-TDP43^{Q331K} mice improves motor phenotypes. **A)** *Prp*-TDP43^{Q331K} x *Stau1*+/- genetic cross and procedures mapped by mouse age in weeks on the experimental timeline. **B)** Results of rotarod behavioral testing at 8, 12, 16 and 20 wks of age by genotype. Values shown are means ± SEM for 3 days of testing when each week of testing. Ns (equal sex ratios) were 18 (WT), 18 (*Stau1*$^{+/-}$), 17 (*Prp*-TDP43^{Q331K}, 8 females, 7 males) and 18 (*Prp*-TDP43^{Q331K};*Stau1*$^{+/-}$), except in week 20 the N for *Prp*-TDP43^{Q331K} was 16 (8 females, 6 males). P-values are shown from mixed-effects ANOVA with the Tukey's test for multiple comparisons, with p-values shown only between WT vs. *Prp*-TDP43^{Q331K} , and *Prp*-TDP43^{Q331K} vs. *Prp*-TDP43^{Q331K};*Stau1*$^{+/-}$. All comparisons between WT and *Stau1*$^{+/-}$ were non-significant. **C)** Forelimb and hindlimb grip strength by genotype for mice 14 and 18 weeks of age. Ns are as in B, with 17 for *Prp*-TDP43^{Q331K}. Values shown for individual mice, and means ± SEM also shown. P-values are shown from mixed-effects ANOVA with the Tukey's test for multiple comparisons. **D)** Heat map showing locomotor behavior by open field testing at 21 wks of age by genotype. Color represents the cumulative, spatially smoothed dwell time at each location, ranging from 0 to 0.5 s. Warmer colors indicate greater occupancy, with red denoting values at or above the 0.5 s display maximum. **E)** Open field measures for, left to right: total

distance travelled, number of entries to the center zone, and distance travelled in the center zone. Values shown for individual mice, and means ± SEM also shown. One-way ANOVA was followed by pairwise comparisons using the two-stage Benjamini–Krieger–Yekutieli procedure to control the false discovery rate at 5% (q = 0.05). Mouse weights, rotarod by sex, open field head turn angle and clasping data are shown in Supplemental Fig. 1.

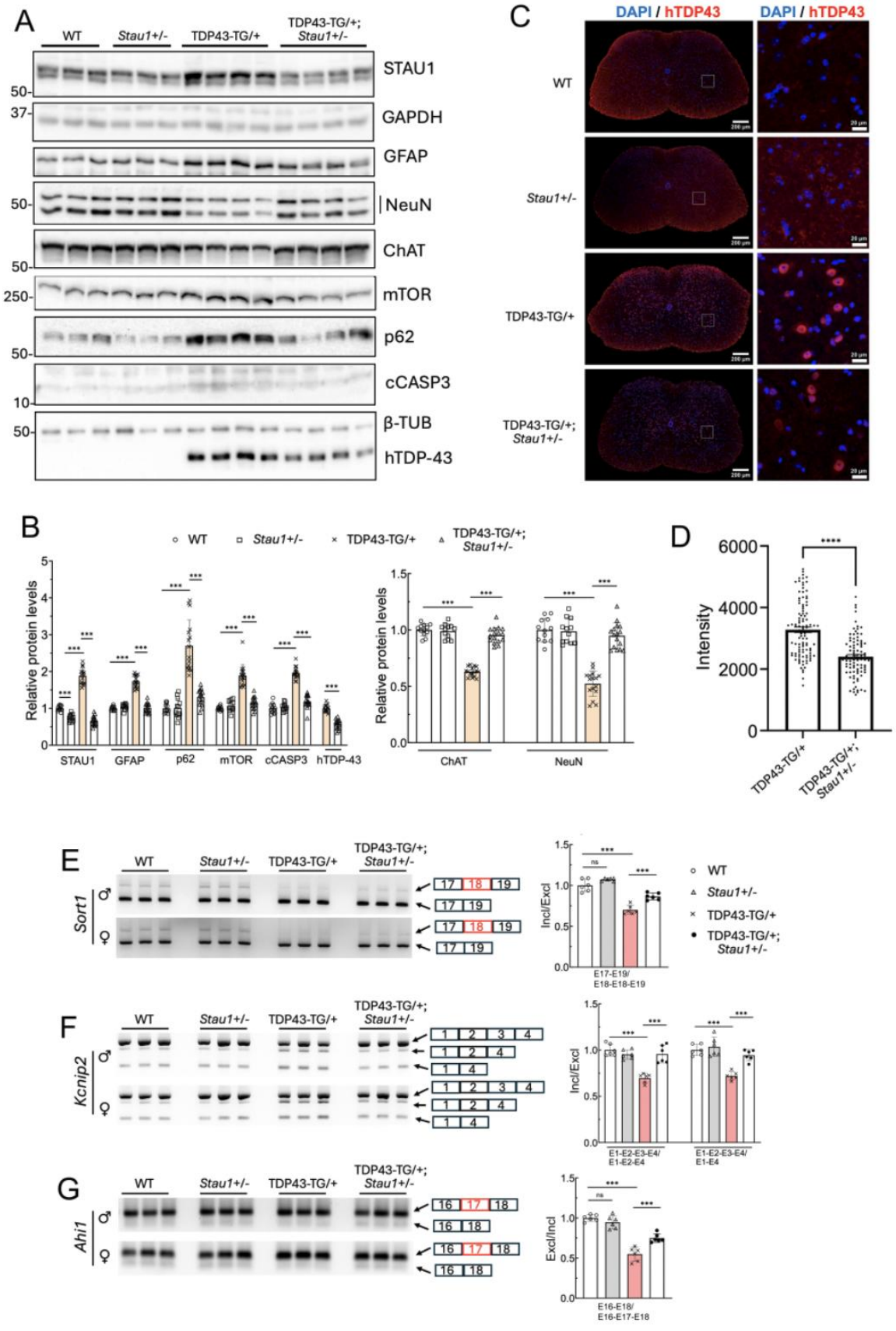

A
WT
Stau1+/-
TDP43-TG/+
TDP43-TG/+; Stau1+/-
STAU1
GAPDH
GFAP
NeuN
ChAT
mTOR
p62
cCASP3
β-TUB
hTDP-43
50-
37-
50-
50-
250-
50-
10-
50-
C
DAPI / hTDP43
DAPI / hTDP43
WT
Stau1+/-
TDP43-TG/+
TDP43-TG/+; Stau1+/-
B
WT
Stau1+/-
TDP43-TG/+
TDP43-TG/+; Stau1+/-
Relative protein levels
STAU1
GFAP
p62
mTOR
cCASP3
hTDP-43
ChAT
NeuN
D
Intensity
6000
4000
2000
0
****
TDP43-TG/+
TDP43-TG/+; Stau1+/-
E
Sort1
WT
Stau1+/-
TDP43-TG/+
TDP43-TG/+; Stau1+/-
Incl/Excl
E17-E19/
E18-E18-E19
F
Kcnip2
E1-E2-E3-E4/
E1-E2-E4
E1-E2-E3-E4/
E1-E4
G
Ahi1
Excl/Incl
E16-E18/
E16-E17-E18

Fig. 2. Genetic reduction of *Stau1* in *Prp*-TDP43^{Q331K} (TDP43-TG/+) mice improves molecular, histological, and TDP-43-dependent splicing phenotypes. Endpoint analyses were performed in a prespecified subset of mice from Fig. 1. **A,B)** Western blot analysis of the indicated proteins in spinal cord lysates **(A)** and corresponding quantification **(B)** show that abnormal protein abundance in *Prp*-TDP43^{Q331K} mice is significantly ameliorated by *Stau1* haploinsufficiency. Values are mean ± SD; *n* = 3–4 males and 3–4 females per group. Each lane represents an individual mouse. Representative blots from male mice are shown; corresponding female data are shown in Supplementary Fig. 2. Technical replicates are plotted and were averaged for statistical analysis. One-way ANOVA with Bonferroni's multiple-comparisons test; ***, $P < 0.001$. **C,D)** Immunofluorescent labeling with a human TDP-43–specific antibody **(C)** and quantification of total TDP-43 immunoreactivity within spinal cord motor-neuron regions of interest (ROIs) **(D)** show reduced TDP-43 abundance with *Stau1* haploinsufficiency. Images were contrast-enhanced to facilitate manual delineation of motor-neuron ROIs in the boxed regions indicated on the left; corresponding higher-magnification views are shown on the right; fluorescence quantification was performed on the original, unadjusted images. *n* = 4 mice per group (2 males and 2 females); 105 motor neurons were quantified in *Prp*-TDP43^{Q331K} mice and 91 in *Prp*-TDP43^{Q331K};*Stau1*$^{+/-}$ mice. ****, $P < 0.0001$; two-sided Student's *t*-test. **E**–**G)** RT-PCR analysis using brain hemisphere extracts demonstrates that abnormal splicing of *Sort1* **(E)**, two *Kcnip2* splice variants **(F)**, and *Ahi1* **(G)** in *Prp*-TDP43^{Q331K} mice is significantly ameliorated by *Stau1* haploinsufficiency. Gels from males (top) and females (bottom) are shown. Quantification shows ratios of exon inclusion to exclusion for *Sort1* and *Kcnip2* **(E,F)** and exon exclusion to inclusion for *Ahi1* **(G)**. Values are mean ± SD. *n* = 6 mice per group. One-way ANOVA with Bonferroni's multiple-comparisons test; ***, $P <$ 0.001; ns, not significant.

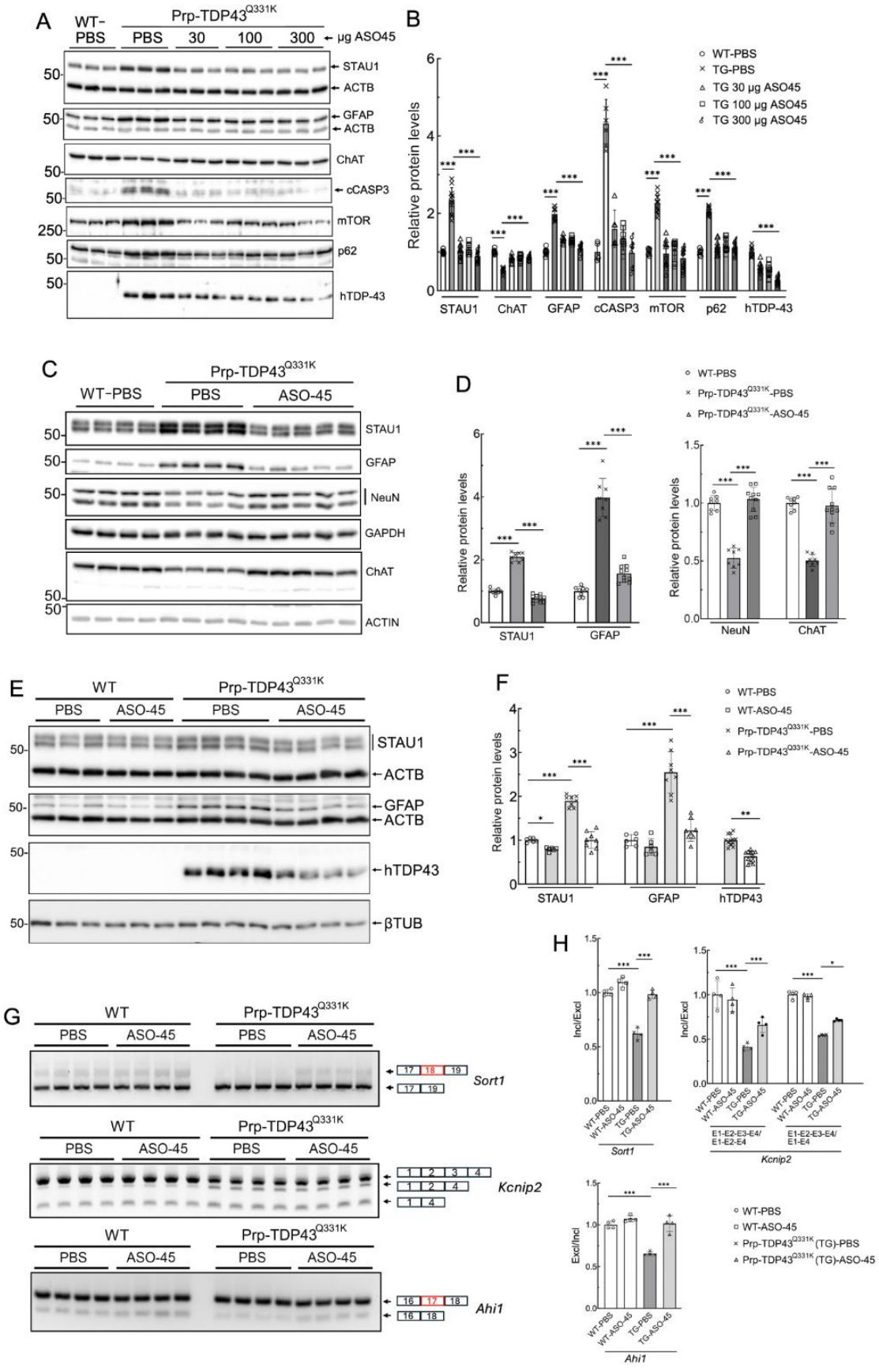

A
WT-PBS
Prp-TDP43Q331K
PBS
30
100
300
µg ASO45
STAU1
ACTB
GFAP
ACTB
ChAT
cCASP3
mTOR
p62
hTDP-43
B
Relative protein levels
WT-PBS
TG-PBS
TG 30 µg ASO45
TG 100 µg ASO45
TG 300 µg ASO45
STAU1
ChAT
GFAP
cCASP3
mTOR
p62
hTDP-43
C
WT-PBS
Prp-TDP43Q331K
PBS
ASO-45
STAU1
GFAP
NeuN
GAPDH
ChAT
ACTIN
D
WT-PBS
Prp-TDP43Q331K-PBS
Prp-TDP43Q331K-ASO-45
Relative protein levels
STAU1
GFAP
NeuN
ChAT
E
WT
Prp-TDP43Q331K
PBS
ASO-45
STAU1
ACTB
GFAP
ACTB
hTDP43
βTUB
F
WT-PBS
WT-ASO-45
Prp-TDP43Q331K-PBS
Prp-TDP43Q331K-ASO-45
Relative protein levels
STAU1
GFAP
hTDP43
G
Sort1
Kcnip2
Ahi1
H
Incl/Excl
Excl/Incl
Sort1
Kcnip2
Ahi1
WT-PBS
WT-ASO-45
TG-PBS
TG-ASO-45
Prp-TDP43Q331K (TG)-PBS
Prp-TDP43Q331K (TG)-ASO-45

Fig. 3. Modification of TDP-43–dependent pathological markers and splicing in the CNS of *Prp*-TDP43^{Q331K} mice treated with ASO-45. A,B) Dose-dependent reduction of STAU1 in spinal cord. **A)** Ten-week-old *Prp*-TDP43^{Q331K} mice received the indicated ASO-45 doses for 2 weeks; spinal cord proteins were analyzed by immunoblotting. ASO-45 significantly reduced STAU1 and altered levels of ChAT, GFAP, cleaved caspase-3 (cCASP), mTOR, p62, and TDP-43. **B)** Quantification of three replicate blots; ***, $P < 0.001$, one-way ANOVA. **C,D)** Reduction of STAU1 in motor cortex. Eight-week-old *Prp*-TDP43^{Q331K} mice received 40 µg ASO-45 for 6 weeks. **C)** Immunoblots show elevated STAU1 in *Prp*-TDP43^{Q331K} mice versus WT littermates and ASO-45–associated changes in GFAP, NeuN, and ChAT. **D)** Quantification of three replicate blots; ***, $P < 0.001$, one-way ANOVA. Each lane represents one mouse; $N = 3–4$ mice. **E–H)** Molecular and splicing changes in cerebral hemispheres. *Prp*-TDP43^{Q331K} mice and WT littermates received PBS or 250 µg ASO-45 at 12 weeks and were analyzed at 26 weeks. **E,F)** Representative immunoblots (**E**) and quantification (**F**) show elevated STAU1 in *Prp*-TDP43^{Q331K} mice, with significant reduction after ASO-45. ASO-45 also reduced STAU1 in WT mice, normalized GFAP in *Prp*-TDP43^{Q331K} mice, and reduced human TDP-43^{Q331K}. ACTB controlled STAU1 and GFAP; βTUB controlled hTDP-43Q331K. $N = 3–4$ mice/group. **G,H)** Representative RT-PCR products (**G**) and quantification (**H**) of TDP-43–dependent splicing of *Sort1, Kcnip2,* and *Ahi1*. Exon-included and -excluded products are shown schematically. Relative to WT controls, *Prp*-TDP43^{Q331K} mice showed greater exclusion of *Sort1* exon 18, *Kcnip2* exon 3 and the *Kcnip2* exon 2–3 cassette, and greater inclusion of *Ahi1* exon 17; ASO-45 significantly reversed these changes. $N = 4$ mice/group from the **E,F** cohort; Western blot sample size was limited by gel capacity. One-way ANOVA with Bonferroni correction: *, $P < 0.05$; **, $P < 0.01$; ***, $P < 0.001$.

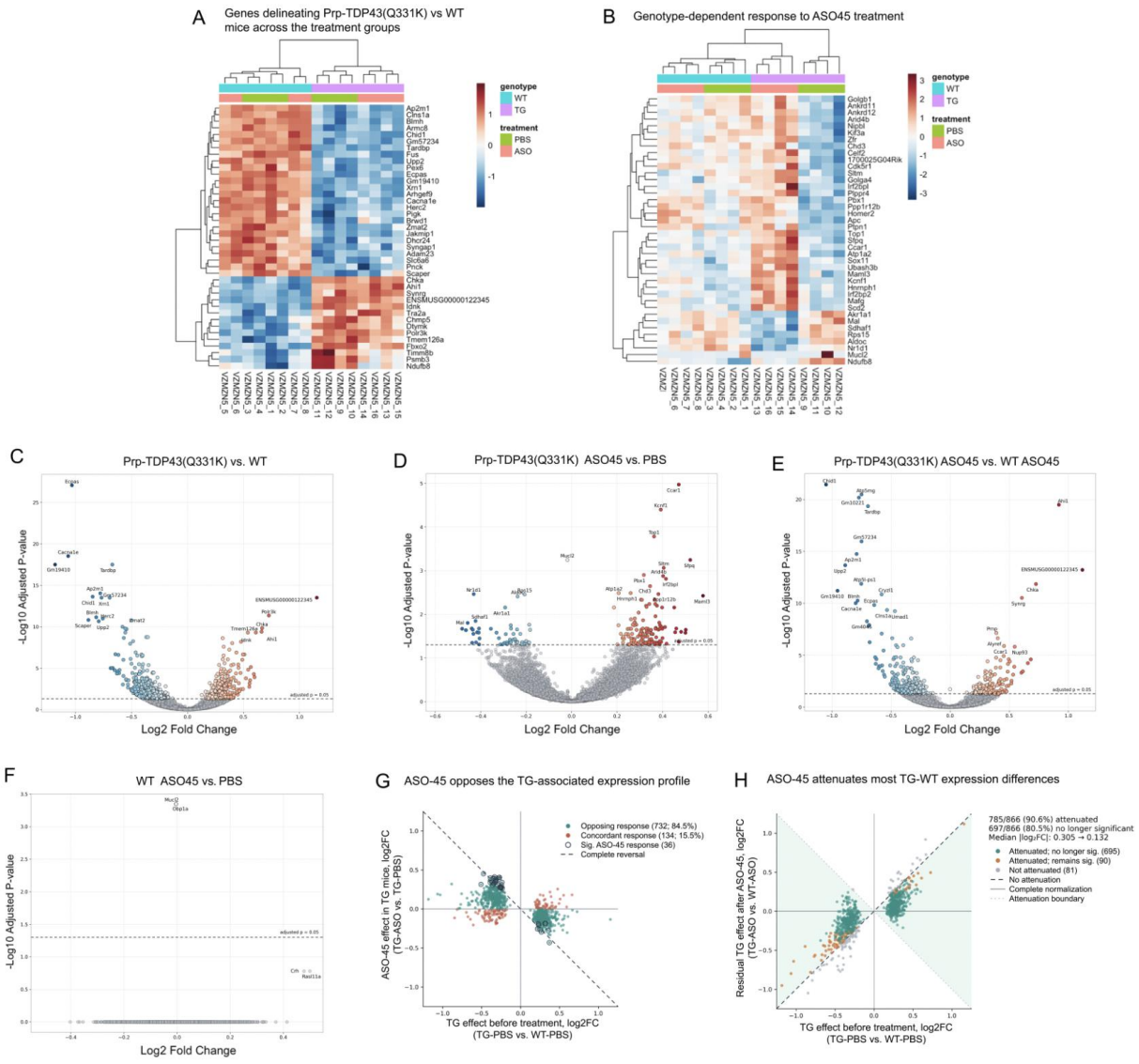


Fig. 4. ASO-45 broadly attenuates the transcriptomic phenotype of *Prp*-TDP-43^{Q331K} mice. RNA sequencing was performed on frontal cortex from wild-type (WT) and *Prp*-TDP-43^{Q331K} transgenic (TG) mice treated with PBS or ASO-45 (*N* = 4 mice/group); this cohort was also analyzed in Fig. 3E–H. **A,B)** Heatmaps show the 40 DEGs with the smallest FDR-adjusted *P* values in each comparison, with hierarchical clustering of genes and samples. Annotation bars indicate genotype and treatment; color represents row-scaled expression (red, higher; blue, lower). **A)** Top DEGs in TG-PBS vs. WT-PBS displayed across all four experimental groups. **B)** Top DEGs in TG-ASO vs. TG-PBS, with WT samples shown for comparison. **C–F)** Volcano plots depict differential expression in PBS-treated TG vs. WT mice (**C**), ASO-45- vs. PBS-

treated TG mice (**D**), ASO-45-treated TG vs. WT mice (**E**), and ASO-45- vs. PBS-treated WT mice (**F**). In **C–F**, each point represents a gene; x-axis, $\log_2$ fold change; y-axis, $-\log_{10}$ (adjusted *P* value). Color indicates direction and magnitude of change; selected genes are labeled. Only two genes were significantly altered in WT mice, indicating minimal detectable off-target transcriptional effects of ASO-45 on the WT transcriptome. **G,H)** Fold-change comparison plots evaluate reversal and attenuation among the 866 DEGs in TG-PBS vs. WT-PBS (adjusted $P < 0.05$). **G)** Untreated TG–WT $\log_2$ fold change is plotted against the ASO response in TG mice (TG-ASO vs. TG-PBS). ASO-45-induced changes opposed the untreated TG phenotype for 732 genes (84.5%; teal); 134 changed in the same direction (15.5%, coral). Black outlines indicate the 36 genes significantly altered by ASO-45 in TG-ASO vs. TG-PBS (adjusted $P < 0.05$), all in the opposing direction. Dashed diagonal indicates complete reversal. **H)** The untreated TG–WT $\log_2$ fold change is plotted against the TG-WT difference after treatment. Shaded areas denotes attenuation (smaller absolute TG–WT fold change after treatment). Overall, 785 genes (90.6%) were attenuated: 695 were no longer significant (teal) and 90 remaining significant (orange). 81 were not attenuated (gray). The median absolute TG–WT $\log_2$ fold change decreased from 0.305 to 0.132. Diagonal, no change; horizontal line, complete normalization.

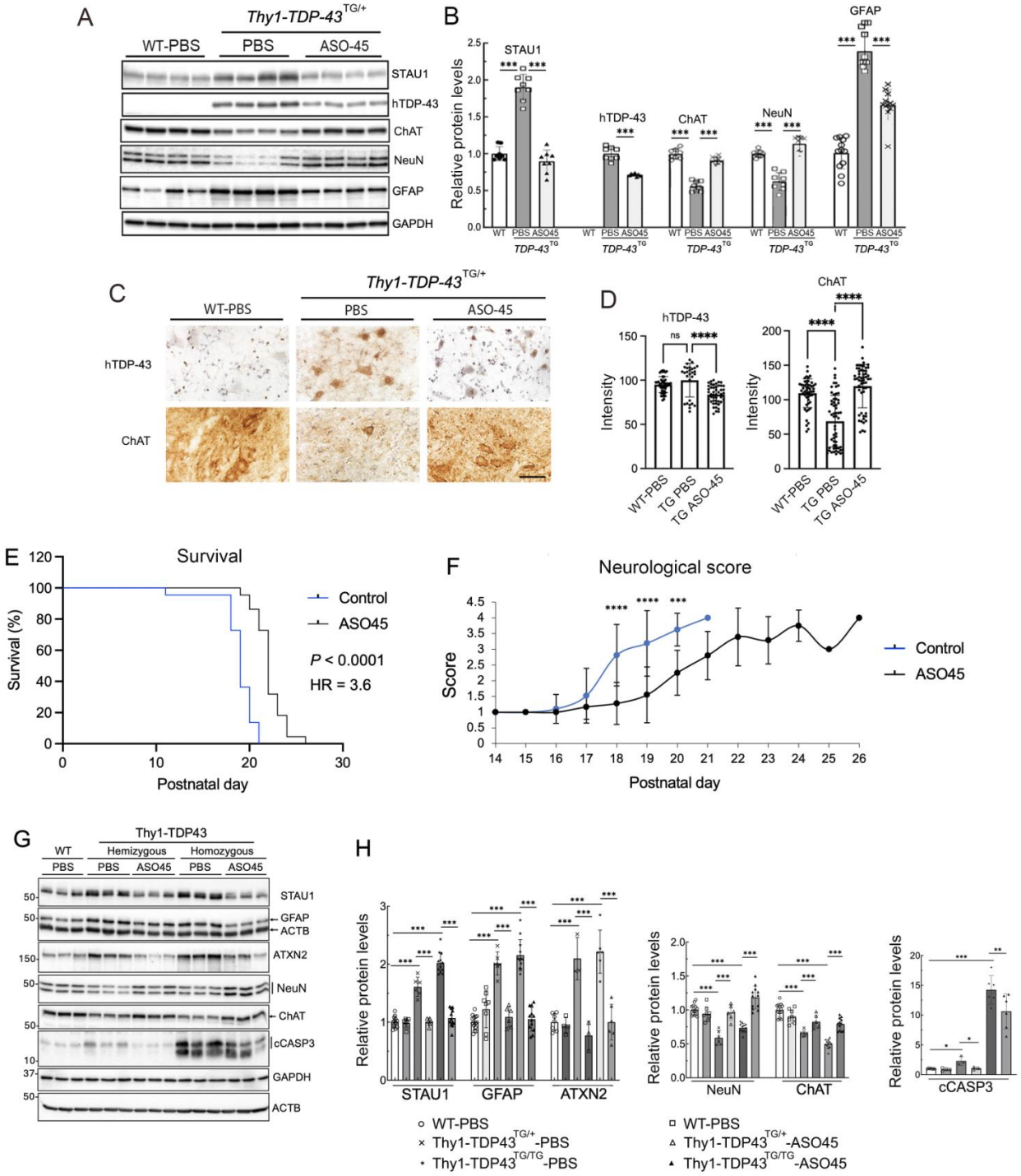
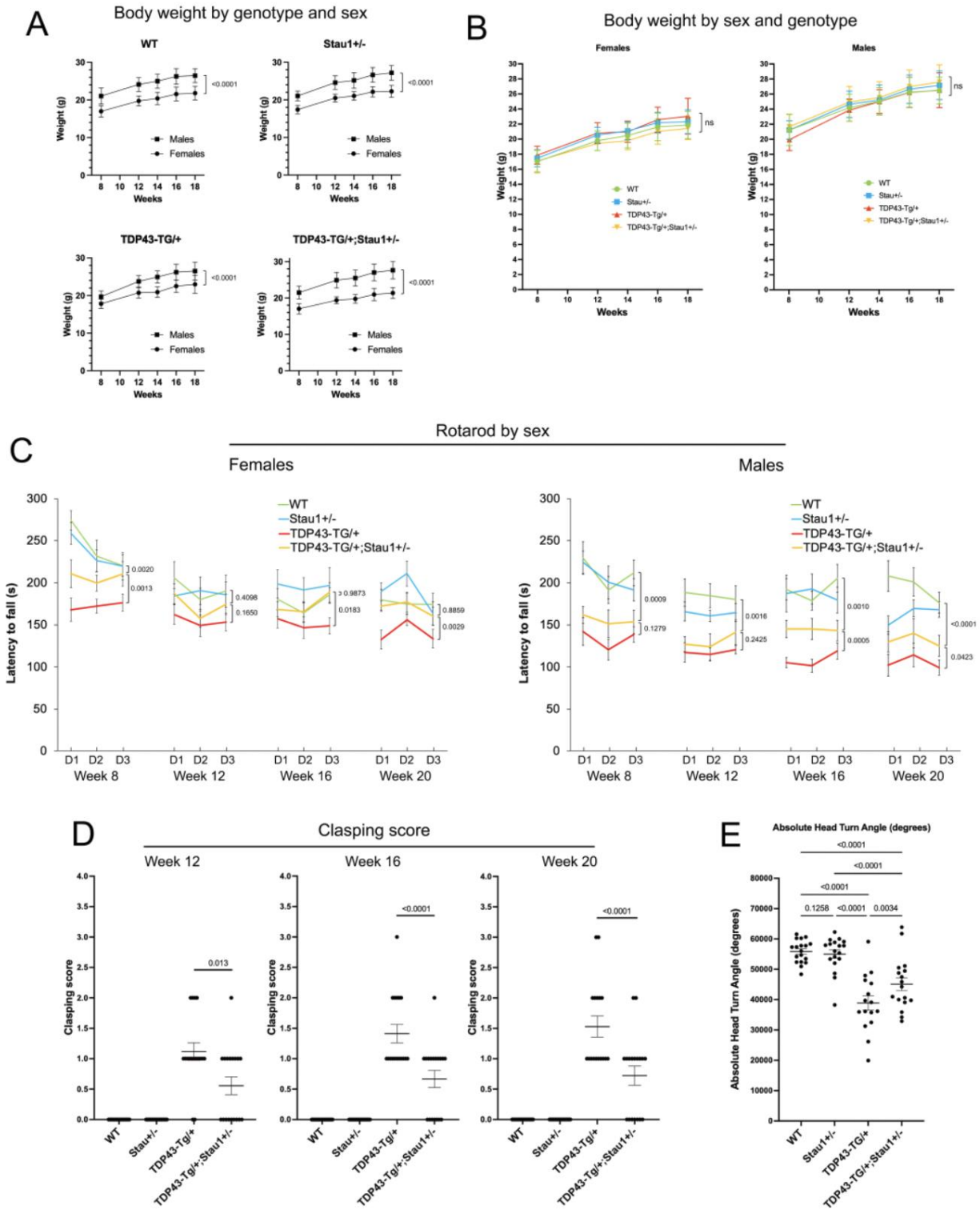


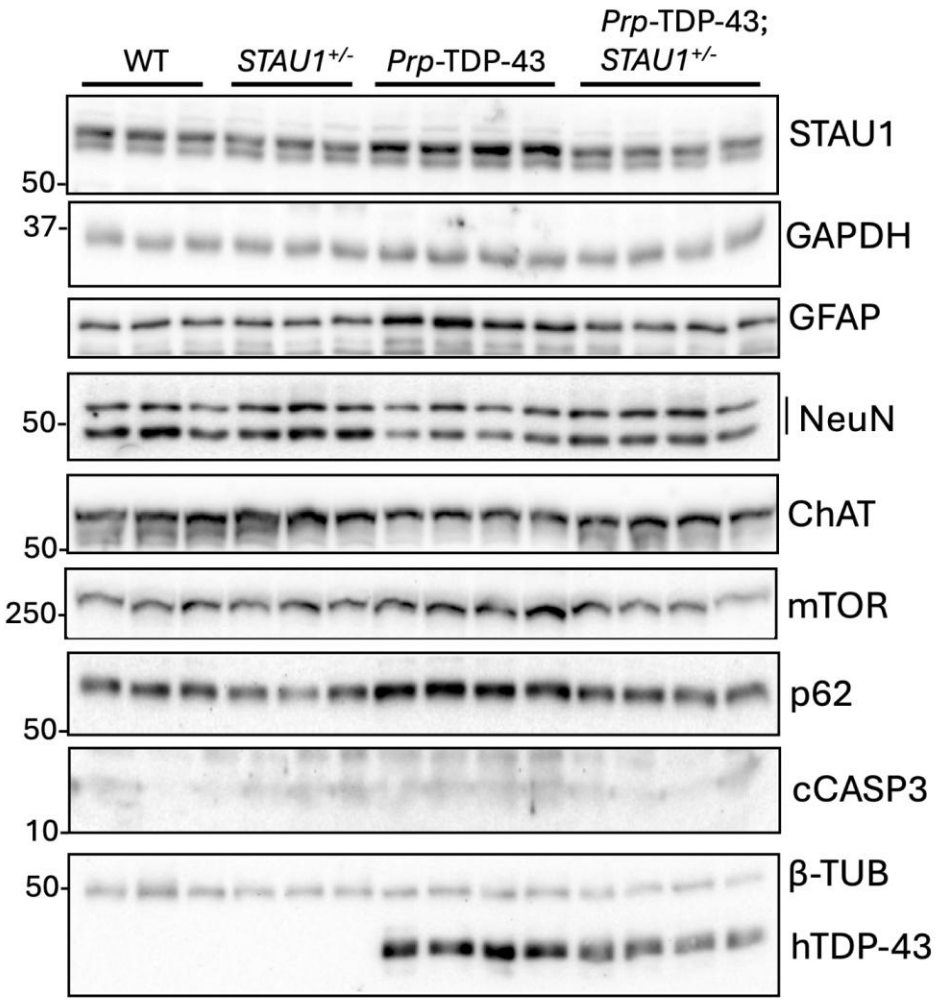
Fig. 5. ASO-45 effects on pathological markers and survival in *Thy1*-TDP-43 transgenic mice. A,B) *Thy1*-TDP-43$^{TG/+}$ mice (24 weeks old) received 300 µg ASO-45 or PBS for 2 weeks. Total spinal cord extracts were analyzed by western blotting for human TDP-43 (hTDP-43), ChAT, NeuN, and GFAP, normalized to GAPDH **(A)**; **B** shows quantification of two blots. **C,D)** Immunohistochemistry of spinal cord TDP-43 and ChAT. **C)** TDP-43 staining was increased in

motor neurons (MNs) of *Thy1*-TDP-43$^{TG/+}$ versus WT mice and reduced by ASO-45. ChAT staining was reduced in TG MNs and increased by ASO-45. Objective, 40x; scale bar, 50 μm. **D)** TDP-43 and ChAT staining intensity per MN. *P* values were determined by one-way ANOVA with Bonferroni correction: $P < 0.05$; $^{**}P < 0.001$; $^{***}P < 0.0001$. **E–H)** Reducing STAU1 in homozygous *Thy1*-TDP-43$^{TG/TG}$ mice (C57BL/6J background) increased survival and improved molecular phenotypes. Mice received 10–30 μg ASO-45 or vehicle by ICV injection at P1–P3 (*n* = 22/group). **E)** Kaplan–Meier survival analysis. Log-rank *P* value and hazard ratio (HR) are shown. Mean survival was 19 days with vehicle and 22 days with ASO-45, a 15.7% increase. **F)** Neurological scores were lower in ASO-45–treated than vehicle-treated *Thy1*-TDP-43$^{TG/TG}$ mice. Mean ± SD; two-way ANOVA with Bonferroni post hoc correction: $^{***}P < 0.0001$. **G,H)** Endpoint brain western blots **(G)** and quantification **(H)** for mice in E,F. Blots also included vehicle-treated WT mice (WT-PBS) and vehicle- or ASO-45–treated *Thy1*-TDP-43$^{TG/+}$ mice. Elevated STAU1 in hemizygous and homozygous TG mice was accompanied by elevated ATXN2 and GFAP and reduced ChAT and NeuN; these abnormalities were normalized by ASO-45. Cleaved CASP3 was normalized in ASO-45–treated hemizygous mice. In homozygous mice, markedly elevated cleaved CASP3 was reduced by ~23%. Blots including ASO-45–treated WT mice are shown in Supplementary Fig. 14. *P* values were determined by one-way ANOVA with Bonferroni correction: $P < 0.05$; $^{*}P < 0.01$; $^{**}P < 0.001$.

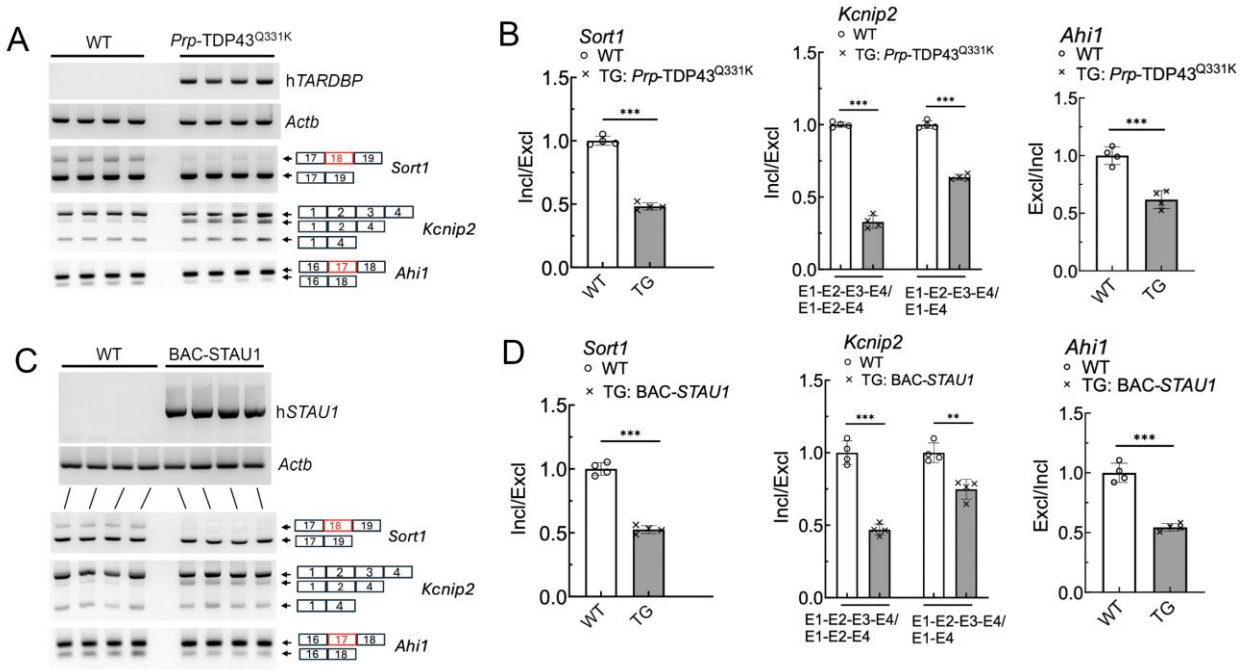
Supplementary Information



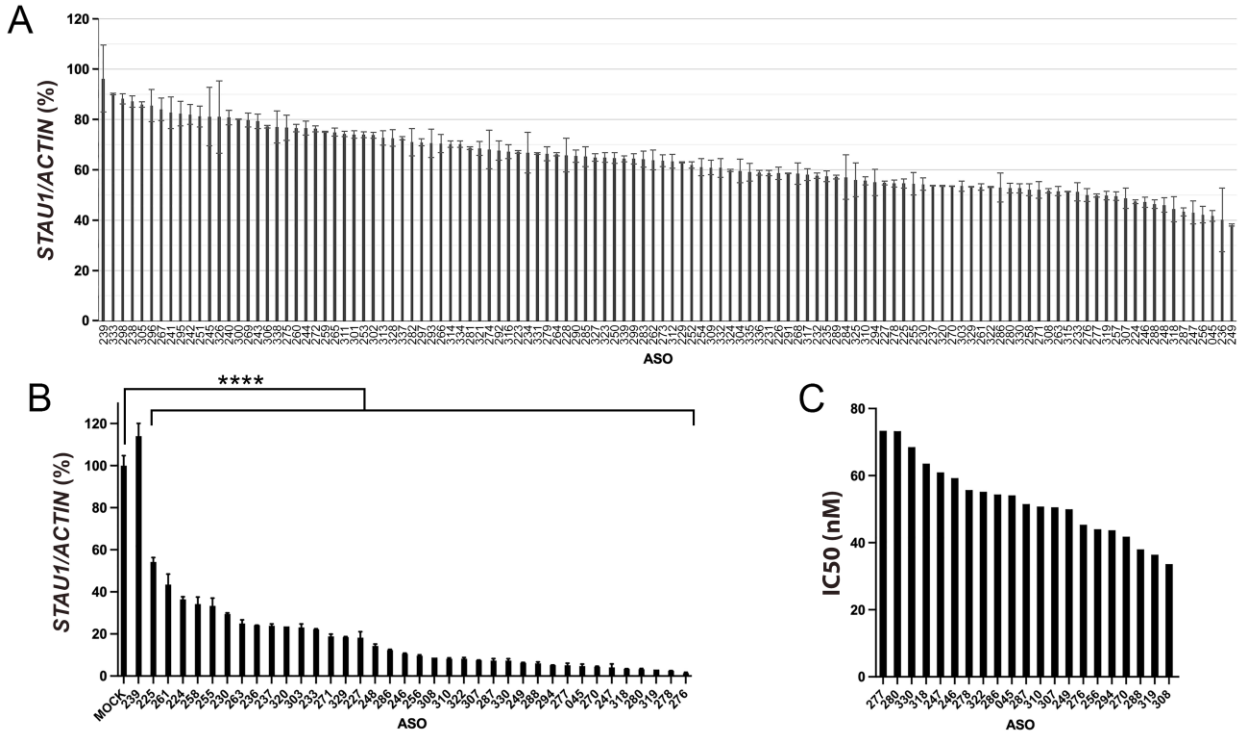
Supplementary Fig. 1. *Prp*-TDP43-Q331K/+ x *Stau1*$^{+/-}$ genetic interaction study: Body weights and rotarod by sex, open field head turn angle and clasping scores. A, B) Body weight by genotype and sex with age. **A)** Male and female weights shown separately within each genotype. Values are means ± SD. **B)** Genotype groups compared separately in females and males. Values are means ± SD. **C)** Results of rotarod behavioral testing at 8, 12, 16 and 20 wks of age by sex and genotype. Values shown are means ± SEM for 3 days of testing when each week of testing. For females, all group Ns are 8. For males, Ns were 8 (WT), 8 (*Stau1*$^{+/-}$), 7 (*Prp*-TDP43^{Q331K}) and 8 (*Prp*-TDP43^{Q331K};*Stau1*$^{+/-}$), except in week 20 the N for *Prp*-TDP43^{Q331K} was 6. P-values are shown from mixed-effects ANOVA with the Tukey's test for multiple comparisons, with p-values shown only between WT vs. *Prp*-TDP43^{Q331K} , and *Prp*-TDP43^{Q331K} vs. *Prp*-TDP43^{Q331K};*Stau1*$^{+/-}$. All comparisons between WT and *Stau1*$^{+/-}$ were non-significant. **D)** Clasping scores at 12, 16 and 20 wks of age. Ns match those reported in Fig. 1 for rotarod testing in wks 12, 16 and 20. Values are means ± SD. P-values are indicated. **E)** Absolute head turn angle, a measure of exploration, determined from open field behavioral testing. Values shown for individual mice, and means ± SEM also shown. One-way ANOVA was followed by pairwise comparisons using the two-stage Benjamini–Krieger–Yekutieli procedure to control the false discovery rate at 5% (q = 0.05).



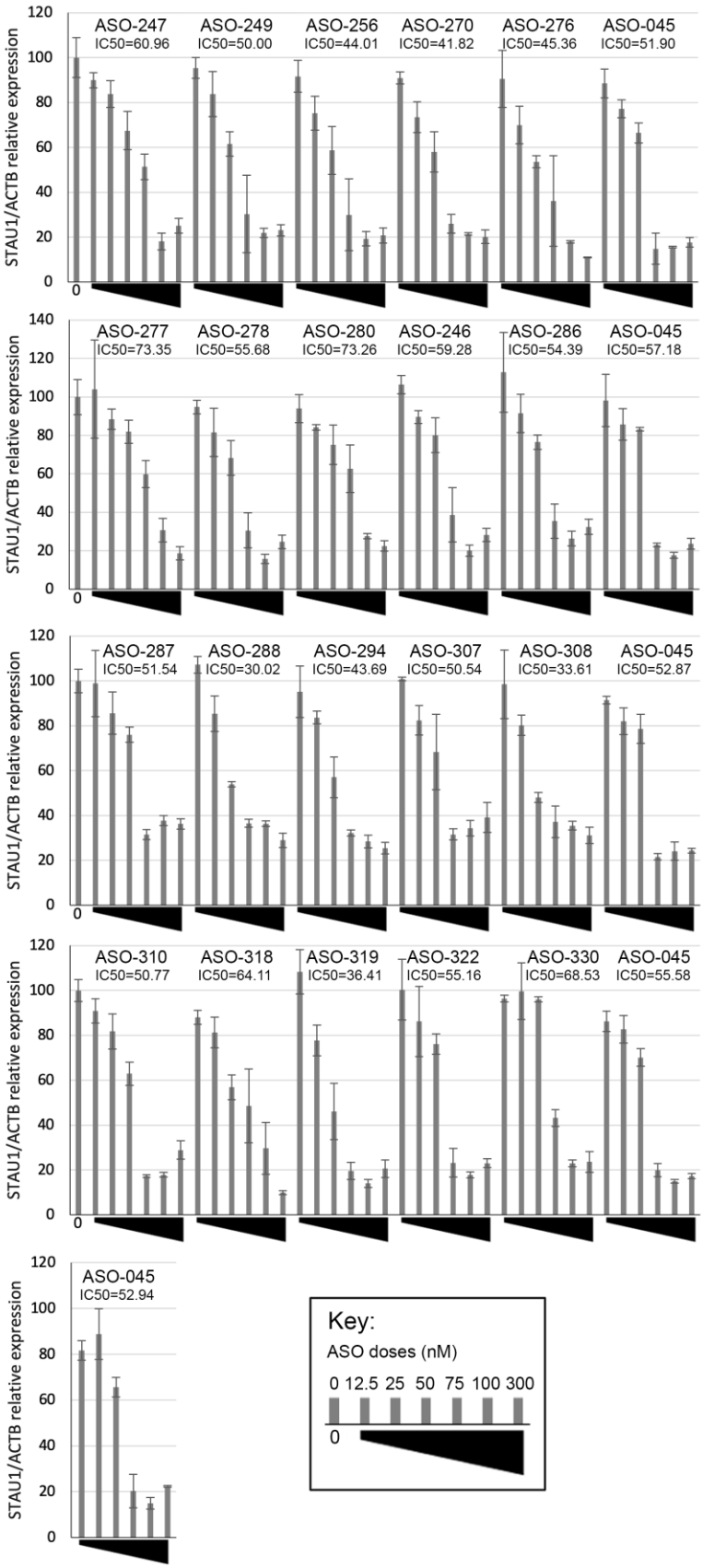
Supplementary Fig. 2. Genetic reduction of *Stau1* ameliorates molecular abnormalities in female *Prp*-TDP43^{Q331K} (TG) mice. Western blot analysis of the indicated proteins in spinal cord lysates from female mice, corresponding to the male blots shown in Fig. 2A. Each lane represents an individual mouse; *n* = 3–4 females per group. Quantification of combined male and female data is shown in Fig. 2B and demonstrates that abnormal protein abundance in *Prp*-TDP43^{Q331K} mice is significantly ameliorated by *Stau1* haploinsufficiency.



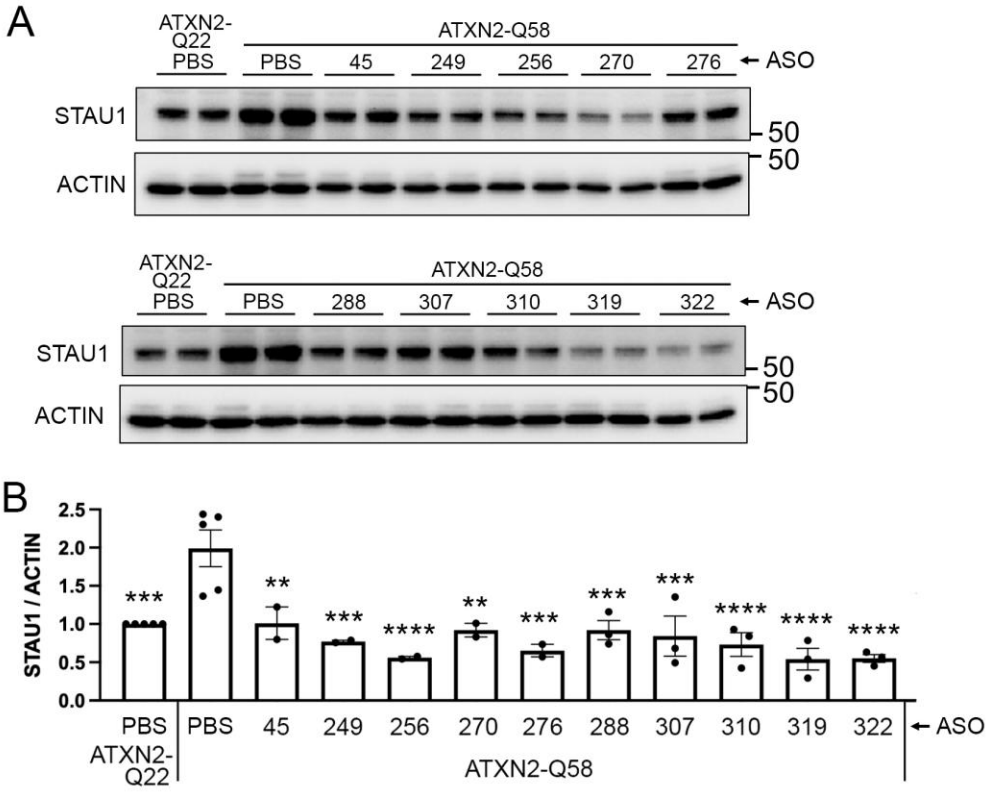
Supplementary Fig. 3. Similarity of TDP-43–dependent splicing alterations in spinal cord of *Prp*-TDP43^{Q331K} and BAC-STAU1 mice. TDP-43–dependent alternative splicing was assessed by RT-PCR for the spinal cord transcripts *Sort1*, *Kcnip2*, and *Ahi1*. **A,B)** *Prp*-TDP43^{Q331K} mice. Representative RT-PCR products **(A)** showing the abundance of h*TARDBP* in *Prp*-TDP43^{Q331K} mice relative to *Actb*, and exon-included and exon-excluded splice variants by RT-PCR. Exons are indicated schematically. Quantification **(B)** showing increased exon 18 exclusion in *Sort1*, increased exon 3 exclusion as well as exon 2-3 exclusion in *Kcnip2*, and increased exon 17 exclusion in *Ahi1*, in *Prp*-TDP43^{Q331K} mice relative to WT controls. **C,D)** BAC-STAU1 mice. Representative RT-PCR products **(C)** showing the abundance of the h*STAU1* transcript in BAC-STAU1 mice relative to *Actb*, and exon-included and exon-excluded splice variants by RT-PCR. Exons are indicated schematically. Quantification **(D)** showing increased exon 18 exclusion in *Sort1*, increased exon 3 exclusion as well as exon 2-3 exclusion in *Kcnip2*, and increased exon 17 exclusion in *Ahi1*, in BAC-STAU1 mice relative to WT controls. N = 4 mice per group. Statistical analysis was performed using one-way ANOVA with Bonferroni correction. **, $p < 0.01$; ***, $p < 0.001$.



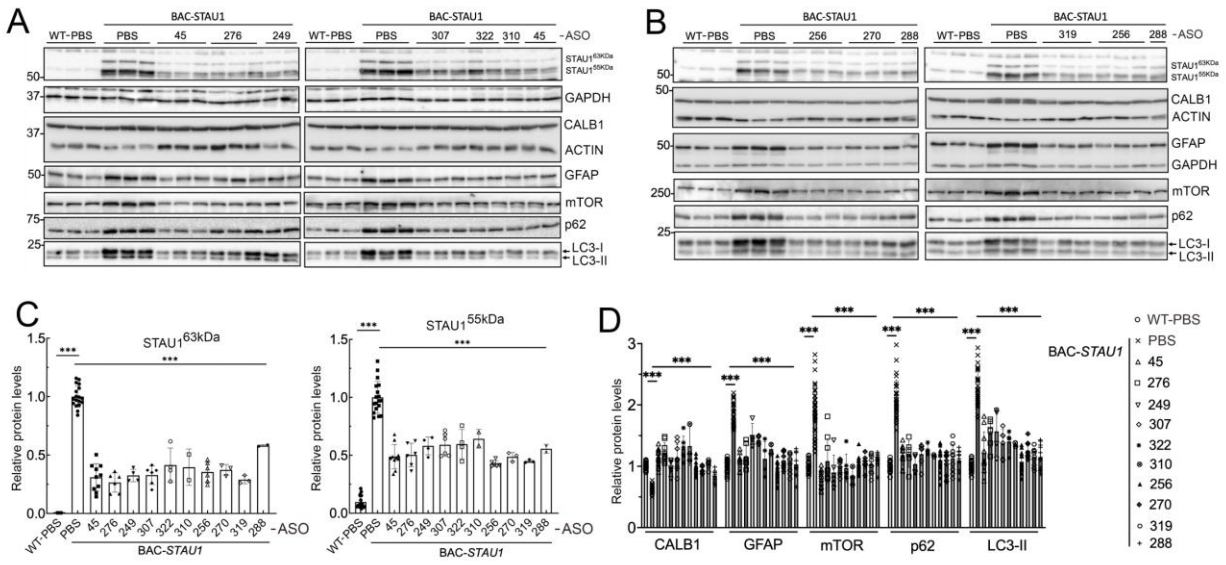
Supplementary Fig. 4. ASO screen, with *STAU1* mRNA levels determined by qPCR. A) 118 STAU1 ASOs from the *in silico* design step were screened in HEK-293 cells in duplicate transfections at 50 nM. The *STAU1/ACTIN* values shown are relative to mock transfected HEK-293 set to 100%, and are mean ± SD for duplicate wells. **B)** A selection of efficacious *STAU1* ASOs from the primary screen were rescreened in SCA2 (Q22/Q45) patient fibroblasts (FBs) in triplicate at 100 nM. A noneffective ASO in **(A)**, ASO-239, was included as a non-targeting control, and did not lower *STAU1* expression in SCA2 FB cells. Values are mean ± SD. All pairwise comparisons to the mock transfected control are significantly different (****, $p<0.0001$), determined by one-way ANOVA with the Tukey correction for multiple comparisons. **C)** IC50s (nM) from 6-point concentration curves for the most efficacious 21 ASOs in B. Charts from which IC50s were derived are shown in Supplementary Data Fig. 5.


ASO-247
IC50=60.96
ASO-249
IC50=50.00
ASO-256
IC50=44.01
ASO-270
IC50=41.82
ASO-276
IC50=45.36
ASO-045
IC50=51.90
ASO-277
IC50=73.35
ASO-278
IC50=55.68
ASO-280
IC50=73.26
ASO-246
IC50=59.28
ASO-286
IC50=54.39
ASO-045
IC50=57.18
ASO-287
IC50=51.54
ASO-288
IC50=30.02
ASO-294
IC50=43.69
ASO-307
IC50=50.54
ASO-308
IC50=33.61
ASO-045
IC50=52.87
ASO-310
IC50=50.77
ASO-318
IC50=64.11
ASO-319
IC50=36.41
ASO-322
IC50=55.16
ASO-330
IC50=68.53
ASO-045
IC50=55.58
ASO-045
IC50=52.94
STAU1/ACTB relative expression
Key:
ASO doses (nM)
0 12.5 25 50 75 100 300
0

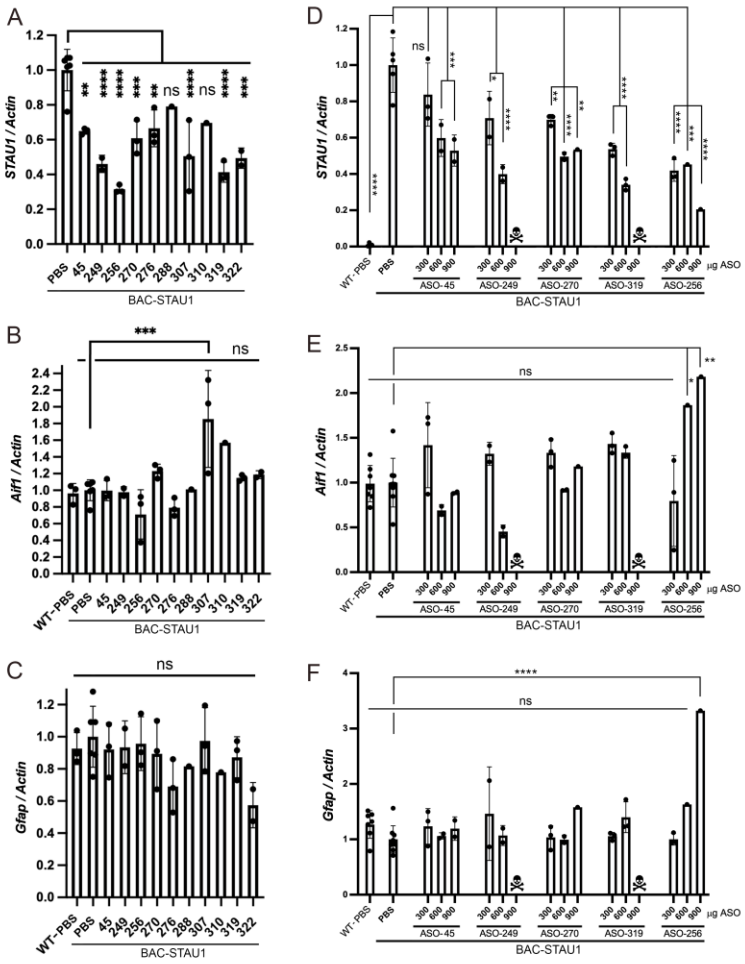
Supplementary Fig. 5. Dose response for lowering *STAU1* expression for 22 ASOs in SCA2 (Q22/Q45) patient derived fibroblast line (SCA2 500-1). Cells were plated in 384 well plates and triplicate wells were included for each ASO dose. STAU1 abundance relative to *ACTB* was determined by qPCR following 48 hours transfection time. Experiments were done in batches with ASO-45 retested on each plate as a comparative control. IC50s were determined using the Hill equation. The value shown for the 0 nM dose is the mean across the five batches. The IC50 mean and SD for ASO-45 is 54.09 ± 2.2 nM.



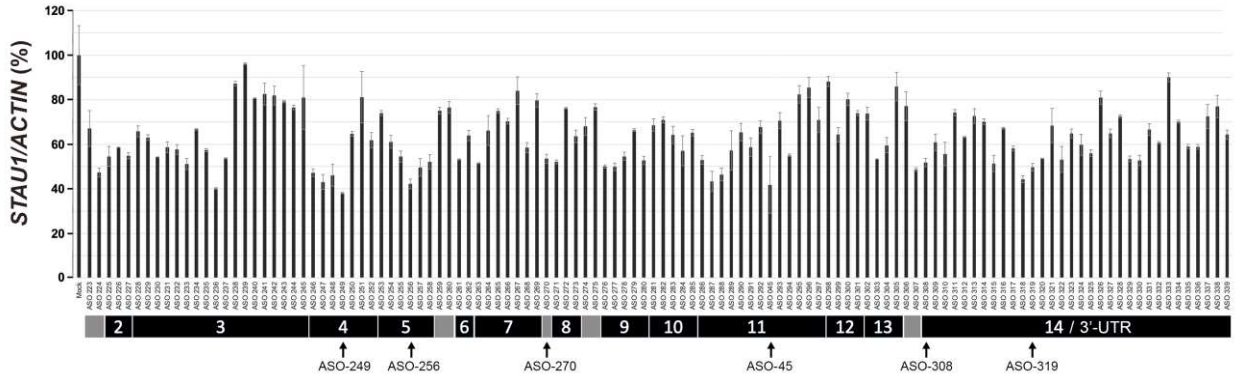
Supplementary Fig. 6. ASO efficacy for lowering STAU1 abundance in HEK-293 ATXN2-Q58 KI cells. A) HEK-293 ATXN2-Q58 KI cells with elevated STAU1 abundance relative to non-mutant HEK-293 ATXN2-Q22 cells were transfected in duplicate cultures with 100 nM of each of 10 lead ASOs as indicated, or PBS. Following 48 hrs, STAU1 levels were determined in cell lysates by western blotting. **B)** Quantifications of the blots shown in **(A)**. Values are means ± SD relative to ACTIN. Blots were performed in duplicate or triplicate. ANOVA with Bonferroni corrected probabilities: **, $p<0.01$; ***, $p<0.001$; ****, $p<0.0001$.



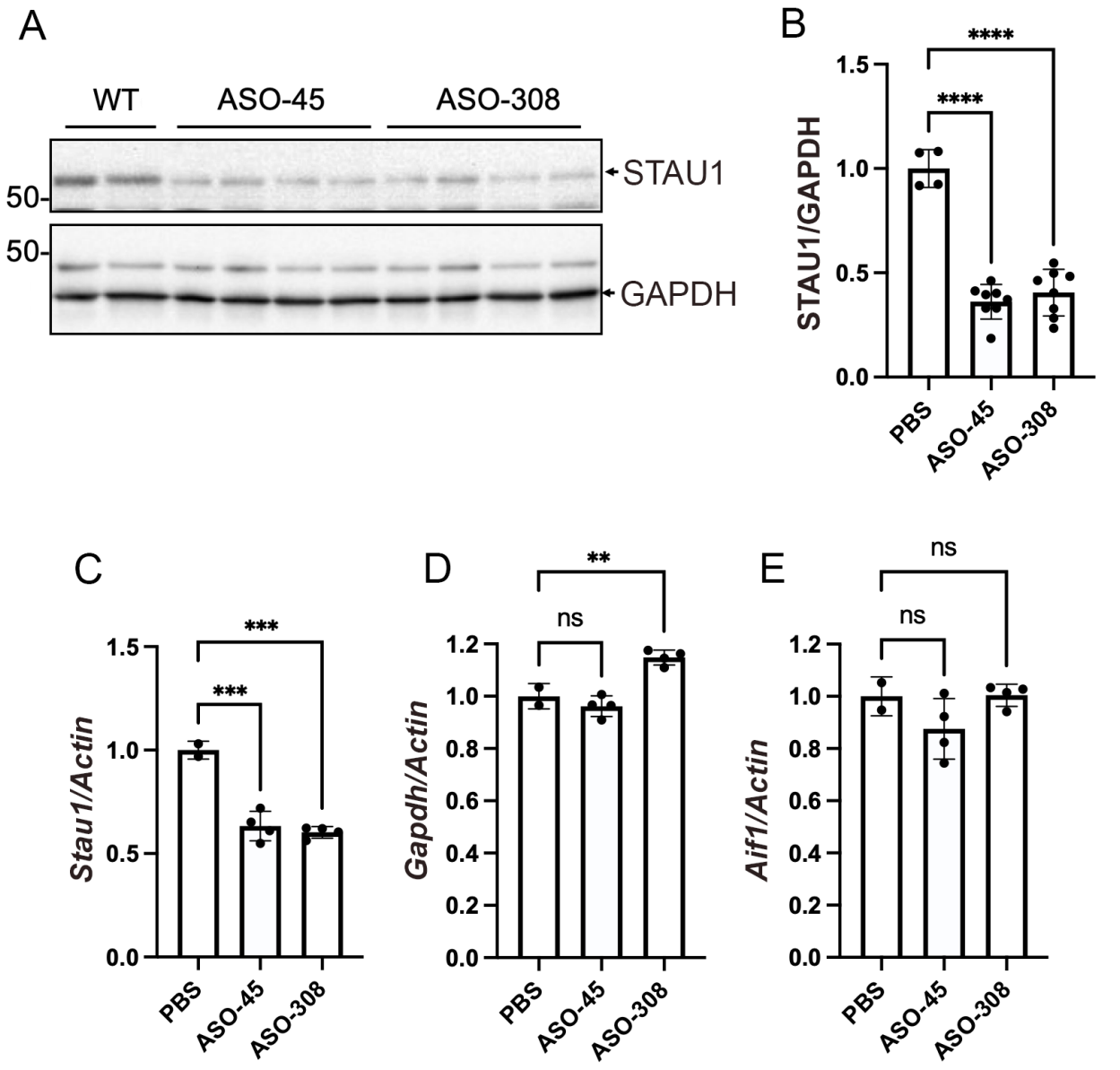
Supplementary Fig. 7. Comparison of the top 10 lead ASOs for lowering STAU1 and modifying autophagy and other disease-related markers in cerebella of BAC-STAU1 mice. BAC-STAU1 mice were injected ICV at 8 weeks of age with 300 μg ASO and evaluated by western blotting for the indicated proteins after 2 weeks, performed in two groups of blots **(A & B)**. Each lane represents a different mouse. **C)** Quantification of the 63 kDa and 55 kDa STAU1 isoforms. **D)** Quantification of CALB1, GFAP, mTOR, p62, LC3-II. Values are means ± SD relative to Actin (for STAU1, CALB1, p62, LC3) or GAPDH (GFAP, mTOR). Blots were performed in duplicate or triplicate. Values are mean ± SD. One-way ANOVA with Bonferroni corrected probabilities: ***, $p<0.001$.



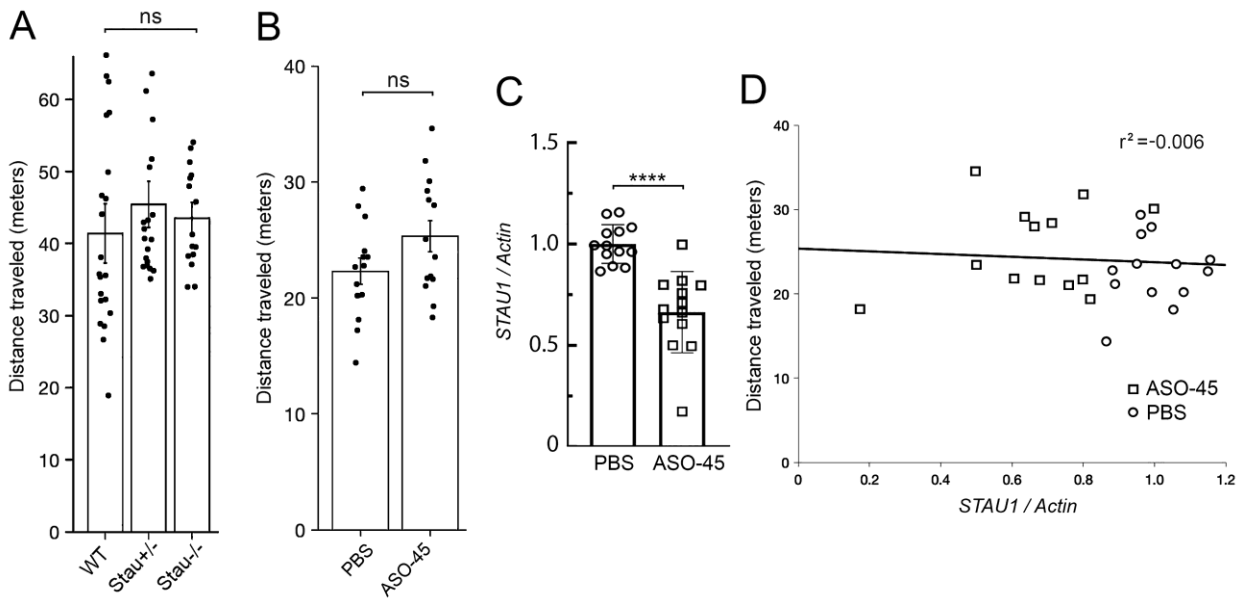
Supplementary Fig. 8. Acute toxicity and gliosis markers *Aif1* and *Gfap* determined by qPCR in spinal cord and cerebella of BAC-STAU1 mice treated with lead ASOs. A–C) Eight wk old mice received a single ICV injection of 300 µg of the indicated ASOs. Two wks after injection, *Stau1*, *Aif1*, and Gfap mRNA levels were measured in spinal cord tissue by qPCR and normalized to *Actb*. **D–F)** Eight wk old mice received ICV injections of the indicated ASOs at the doses shown. Two wks after injection, *Stau1*, *Aif1*, and *Gfap* mRNA levels were measured in cerebellar tissue by qPCR and normalized to *Actb*. Crossed-bones symbols indicate groups with no surviving mice. Data are shown as mean ± SD (n = 3 mice per group). Statistical significance was determined by one-way ANOVA with Bonferroni corrected probabilities: *, p<0.05; **, p<0.01; ***, p<0.001; ****, p<0.0001; ns, not significant.



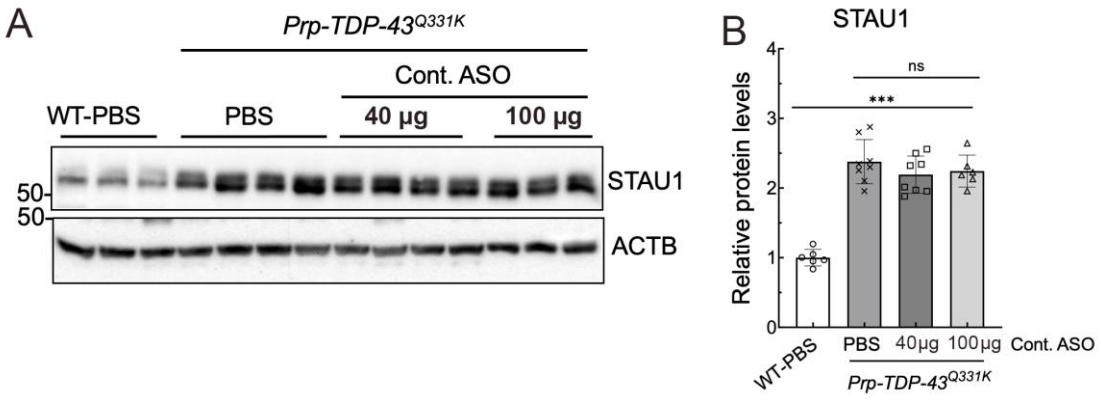
Supplementary Fig. 9. ASOs mapped to *STAU1* exons, with the top 6 leads highlighted using arrows. 118 *STAU1* ASOs were screened in HEK-293 cells in duplicate transfections at 50 nM. The values shown mean ± SD *STAU1/ACTIN* relative to mock transfected HEK-293 set to 100%, determined by qPCR. The chart represents a rearrangement of the data in Fig. 1A. *STAU1* exons and 3'-UTR are indicated. No 5'-UTR or exon1 ASOs were included. Gray boxes represent regions where ASOs crossed a boundary.



Supplementary Fig. 10. ASO-45 and ASO-308 target *Stau1* in WT mice. WT mice were treated at 11 wks of age with 500 μg ASO, and were evaluated for molecular changes at 13 wks of age. N=2 WT injected with PBS and 4 WT mice injected with either ASO-45 or ASO-308. **A,B)** Western blotting of cerebellar protein extracts **(A)** and quantification of duplicate blots **(B)**. Each lane represents a different mouse. **C-E)** Determination of *Stau1* mRNA levels in cerebellar extracts by qPCR **(C)** with evaluation of *Gfap* **(D)** and *Aif1* **(E)**, markers of cytotoxicity. One-way ANOVA with Bonferroni corrected probabilities: **, p<0.01; ***, p<0.001; ****, p<0.0001; ns, not significant.

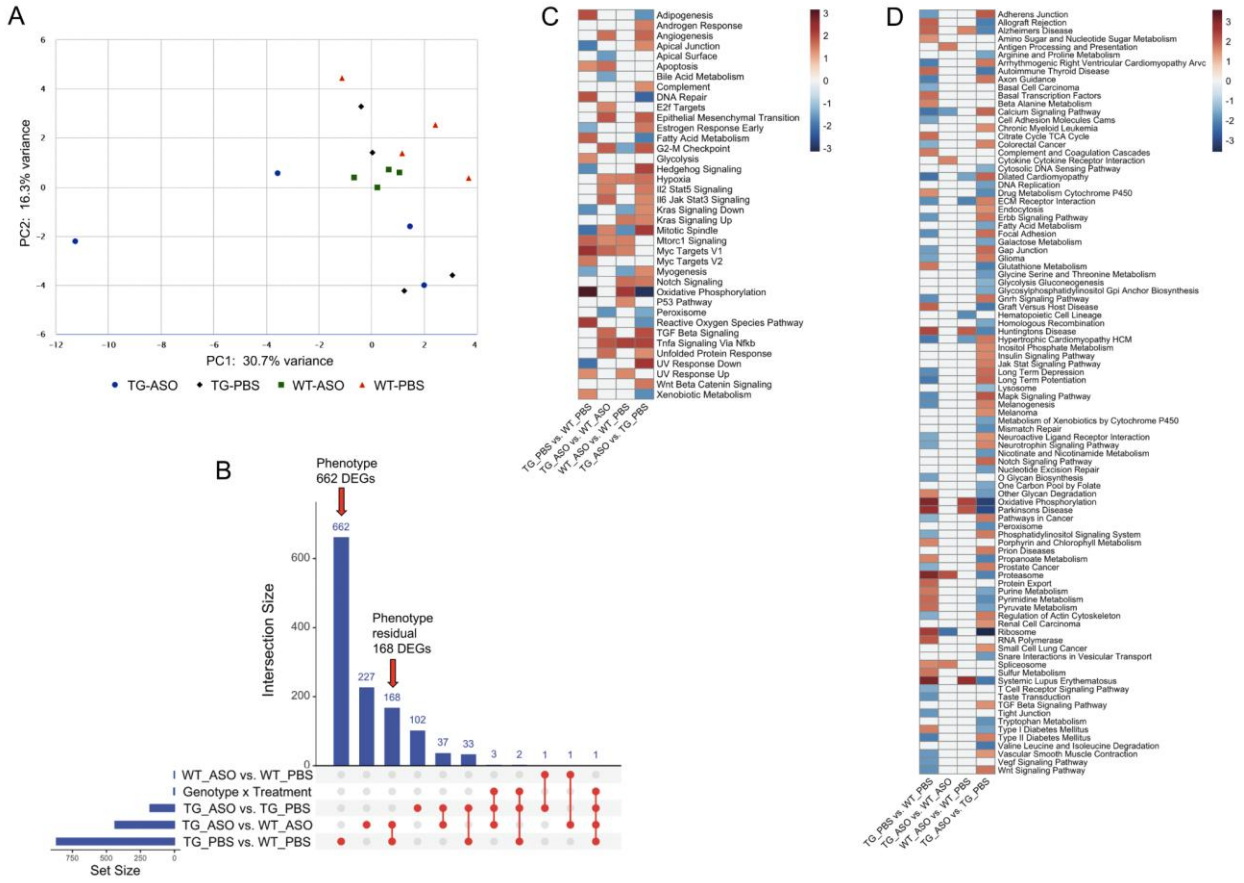


Supplementary Fig. 11. On target open field behavior testing after lowering STAU1 in adult mice. A) Distance travelled as measured by force plate actometry-based center of mass tracking for *Stau1* heterozygous knockout (*Stau1*$^{+/-}$), *Stau1* homozygous knockout (*Stau*1$^{-/-}$) and wildtype littermate mice 6 months of age, recorded over 30 min. No significant difference was observed between groups for genotype or sex (ANOVA, p>0.05). N= 21 WT (10 males 11 females), 20 *Stau1*$^{+/-}$ (10 males 10 females), 15 *Stau1*$^{-/-}$ (8 males 7 females). B-D) WT mice age 3 months treated ICV with 300 μg ASO-45 for 3 wks. **B)** Distance travelled, measured as in A, for center of mass recorded over 10 min (Student's *t*-test, p=0.098). No significant difference was observed between sexes (p>0.05). N=14 mice (7 males 7 females) per group. **C)** Target engagement in brain by qPCR (Student's *t*-test p<0.0001). **D)** Plot of *Stau1* mRNA abundance vs distance revealing no correlation. Pearson's correlation test p=0.73, r=0.078, r^2=-0.006. Values are means ± SEM **(A-B)** or SD **(C)**. Experiments in A & B showed no significant difference in percentage of time in chamber center 50%.



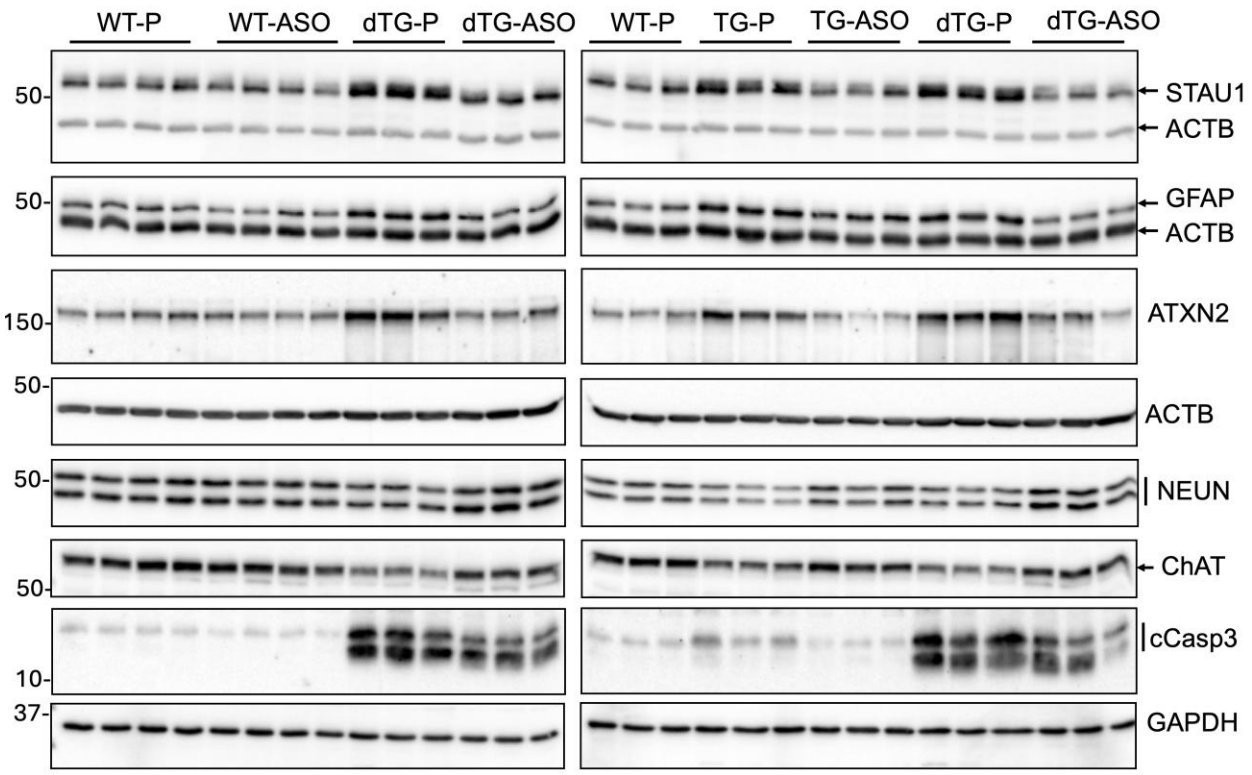
Supplementary Fig. 12. Assessing a non-targeting control ASO for modifying STAU1 abundance in motor cortex. *Prp*-TDP43^{Q331K} mice 20 wks of age were treated with PBS or the indicated doses of the non-targeting control ASO. Age matched wildtype littermates were treated with PBS. Treatments were 6 wks in length.

A) Proteins in motor cortex were evaluated by western blotting. Each lane represents a different mouse. **B)** Quantification of 3 replicate blots. STAU1 was significantly elevated in *Prp*-TDP43^{Q331K} mice compared to WT mice treated with PBS, but no changes with treatment by the non-targeting control ASO were observed. ns, not significant. ***, P<0.001, ANOVA.

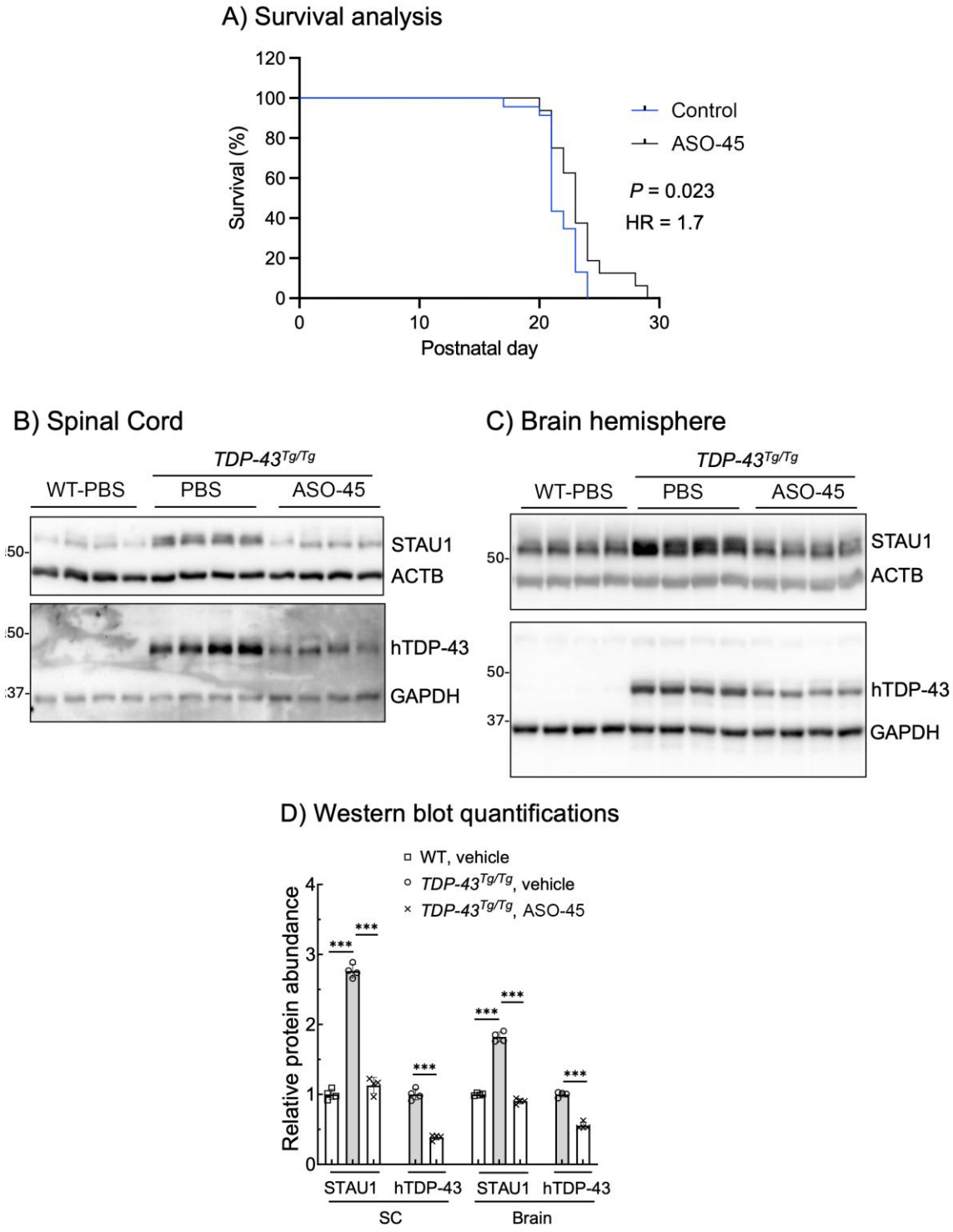


Supplementary Fig. 13. Global and differential transcriptomic analyses of *Prp*-TDP43^{Q331K} mice treated with or without ASO-45. RNA sequencing was performed on frontal cortex from wild-type (WT) and *Prp*-TDP43^{Q331K} transgenic (TG) mice treated with PBS or ASO-45 (N = 4 mice per group). **A)** Principal component analysis (PCA) of transcriptomic profiles from individual mice. Symbols indicate genotype and treatment group. PC1 and PC2 account for 30.7% and 16.3% of the total variance, respectively. **B)** UpSet plot showing unique and overlapping differentially expressed genes (DEGs) across the indicated genotype and treatment comparisons. Horizontal bars indicate the total number of DEGs in each comparison; vertical bars indicate the number unique to or shared among comparisons, as identified by the connected points below. The untreated TG phenotype comprised 662 unique DEGs, whereas 168 DEGs were shared between the untreated and residual post-treatment TG–WT comparisons. DEG intersections do not account for the direction or magnitude of expression changes. **C,D)** Gene set enrichment analysis across the indicated genotype and treatment comparisons using **C)** Hallmark and **D)** KEGG pathway gene sets. Color represents the

normalized enrichment score, with red indicating positive enrichment and blue indicating negative enrichment; white indicates no significant enrichment.



Supplementary Fig. 14. Western blots demonstrating modification of molecular phenotype in brain of *Thy1*-TDP43 mice treated with ASO-45 at the survival study endpoint. WT (wildtype littermates), TG (*Thy1*-TDP43$^{TG/+}$), dTG (*Thy1*-TDP43$^{TG/TG}$), P (PBS treated), ASO (ASO-45 treated). These blots supplement those presented in Fig. 5G.



Supplementary Fig. 15. Reduction of STAU1 abundance in *Thy1*-TDP43$^{TG/TG}$ mice increased survival and improved molecular phenotypes (replicate study with mice of background B6;SJL). A) *Thy1*-TDP43$^{TG/TG}$ mice were treated ICV at P3 with vehicle (PBS) (n=23 mice) or 30 µg ASO-45 (n=16 mice), followed by Kaplan-Meier survival analyses using

homozygous *Thy1*-TDP43$^{TG/TG}$ mice. Log-rank test P-value and hazard ratio (HR) are shown. Mean survival was 21 days for vehicle treated and 23 days for ASO treated mice. *Thy1*-TDP-43$^{TG/TG}$ mice receiving ASO-45 had a mean 9.5 % improved survival. **B-D)** Endpoint western blotting and quantifications for mice in A compared to vehicle treated WT littermates, using spinal cord and brain extracts. The result demonstrated elevated STAU1 in *Thy1*-TDP-43$^{TG/TG}$ mice that was significantly normalized by ASO-45. Additionally, TDP-43 was significantly reduced by 66% in SC and ~50% in brain in *Thy1*-TDP-43$^{TG/TG}$ mice treated with ASO-45 compared to mice treated with vehicle. P-values determined by ANOVA with Bonferroni correction: *, $p<0.05$; **, $p<0.01$; ***, $p<0.001$.